Interplay between pair density waves and random field disorders in the pseudogap regime of cuprate superconductors

Cheung Chan
Institute for Advanced Study, Tsinghua University, Beijing, 100084, China
(Received 14 October 2015; revised manuscript received 15 May 2016; published 31 May 2016)

To capture various experimental results in the pseudogap regime of the underdoped cuprate superconductors for temperature $T < T^*$, we propose a four-component pair density wave (PDW) state, in which all components compete with each other. Without random field disorders (RFD), only one of the PDW components survives. If the RFD is included, this state could become phase separated and consist of short range PDW stripes, in which two PDW components coexist but differ in magnitudes, resulting in charge density waves (CDW) and a time-reversal symmetry breaking order, in the form of loop current, as secondary composite orders. We call this phase-separated pair nematic (PSPN) state, which could be responsible for the pseudogap. Using a phenomenological Ginzburg-Landau approach and Monte Carlo simulations, we found that in this state, RFD induces short range static CDW with phase-separated patterns in the directional components, and the static CDW is destroyed by thermal phase fluctuations at a crossover temperature $T_{CO} < T^*$, above which the CDW becomes dynamically fluctuating. The experimentally found CDW with predominantly d-wave form factor constrains the PDW components to have $s' \pm id$-wave pairing symmetries. We also construct a lattice model and compute the spectral functions for the PSPN state and find good agreement with ARPES results.

DOI: 10.1103/PhysRevB.93.184514

I. INTRODUCTION

Since the discovery of the cuprate superconductors [1] (SC), the pseudogap regime has attracted a lot of attentions for its exotic properties [2] and the possible relation to the high temperature d-wave superconductivity (dSC). Two main types of theories are proposed for the pseudogap. One type [3–6] suggests that pseudogap is a precursor to the dSC phase with pre-formed Cooper pairs without global phase coherence. However, mounting experimental evidences are pointing otherwise that pseudogap is indeed another broken symmetry state. The recent inputs mainly come from the x-ray scattering experiments [7–15], which suggest the state is characterized by the onset of incommensurate charge density wave (CDW) with wave vectors at $(\pm 2Q, 0)$ and $(0, \pm 2Q)$, where Q decreases with increasing hole doping. This finding is in accord with earlier scanning tunneling microscope [16–20] (STM) and nuclear magnetic resonance [21,22] (NMR) experiments. There are some early theoretical studies to explain the pseudogap in terms of CDW [23,24]. The phase diagram is however much richer. Other orders associated with different broken symmetries are also detected in the pseudogap, e.g., the time reversal symmetry breaking (TRSB) order detected in polar Kerr rotation [25,26] (PKR) and polarized neutron diffraction [27–30] (PND) experiments and the nematic order [13,31–34] that breaks the C_4 lattice rotational symmetry. This complicated zoo of orders poses a natural question of whether we can unify these into a common origin and understand the pseudogap in a coherent manner. Among the various theories proposed, pair density wave (PDW) order, which is a spatially modulating SC state similar to Fulde-Ferrell-Larkin-Ovchinnikov (FFLO) states [35,36], previously studied in different contexts for the cuprates [37–46], is suggested to be responsible for the pseudogap. Recent works [47,48] by Lee and Agterberg *et al.* have successfully explained many features of the pseudogap. In the PDW theory, the CDW is induced by the PDW as a secondary composite order, accounting for the STM and x-ray scattering results. Moreover, the PDW can also induce a loop current (LC) order [48–50] to account for the TRSB order observed in PKR [25,26] and PND [27–30] experiments. Nonetheless, the PDW order also explain several ARPES features [12,51–55], namely the k_F-k_G misalignment, antinodal gap closing from below, and the Fermi arcs.

Hinted by these successes, the PDW order might hold the key to understand the pseudogap of hole doped cuprates. However, several issues have surfaced. Most noticeably, the charge density waves observed in STM [19,20,56] and REXS [13] are short ranged. STM further show that these density waves form a domain structure and are directional within each domain. The same conclusion is also drawn from REXS. While these results are obtained in no magnetic field, the high field experiments, on the other hand, reveal that the CDW with the same in-plane wave vector is long ranged and unidirectional [21,57–59]. As a first step to understand this onset of long range CDW state at high field [22,58,59], it is essential to explain why the CDW observed in weak field is short ranged.

Experiments however impose stronger constraints, besides the possible order parameters, on theories. Each set of experiments reveals a specific doping dependent temperature scale, but not all these temperature scales can fall into a single simple curve in the phase diagram. This challenges the belief that the pseudogap can be ascribed to a single origin. We shall mention those that are relevant in the current paper. The electronic transport giving rise to linear resistivity [60,61] defines T_ρ that is believed to capture a quantum critical point associated with corresponding order parameter, and it is commonly taken as the definition of the pseudogap temperature scale $T^* \equiv T_\rho$. ARPES measurements define $T_{\text{ARPES}} \sim T^*$, below which unusual quasiparticle spectrum is revealed. Moreover, REXS [7,9,11–15] also found the fluctuating CDW correlation below T^*, but RIXS [8,10] and STM [17] reveal a lower temperature scale $T_{CO} < T^*$ for static charge order. It is found that T_{CO} has a maximum at some

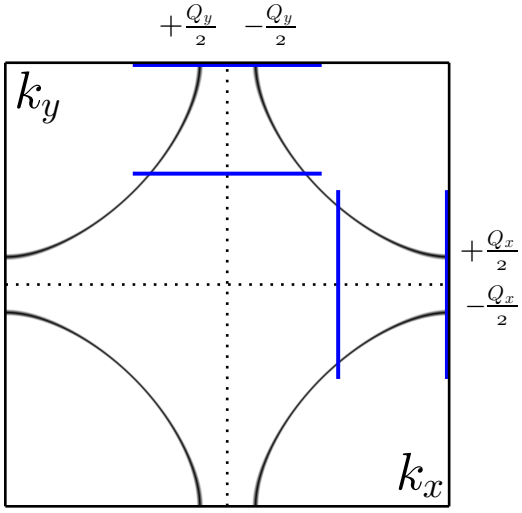

FIG. 1. Bare Fermi surface. The PDW pairing centers $\pm Q_{x,y}/2$ are at the intersections with the Brillouin zone boundary. The blue lines are for the quasiparticle spectral function scans in Figs. 9 and 10.

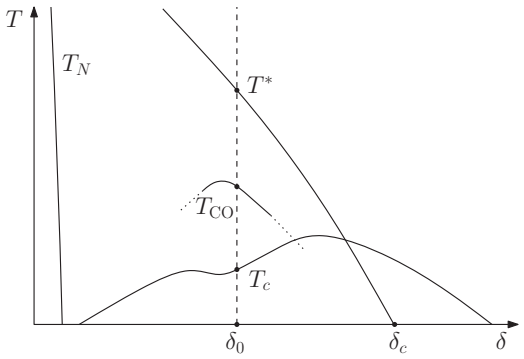

FIG. 2. Schematic phase diagram for hole doped cuprates, where δ is the doping and T is temperature. T^* is the characteristic temperature for the pseudogap, in which we propose the phase-separated pair nematic state is responsible for. T_N is the critical temperature for the antiferromagnetic order near zero doping. Focusing at a doping δ_0 at underdoped regime, T_c is the critical temperature for the dSC, T_{CO} is for the presence of short range static CDW.

doping but T^* decreases as doping increases. A valid theory would be able to explain the emergence of these temperature scales within the pseudogap. Similar to T_{CO}, we note that for TRSB order, there are also two distinct temperature scales found in PND [27–29] (see also Ref. [30]) and PKR [25,55] (see also Ref. [26]) experiments. The PND experiments found that below $T_M \sim T^*$ an intraunit cell (IUC) TRSB magnetic order exists, while the PKR experiments, which also detect TRSB, reveal a strictly lower temperature scale $T_K < T_M$ but doping dependence of T_K shows a similar trend as T_M. However, we shall address the issue of T_K elsewhere.

Motivated by these issues, we study the effect of random field disorders [62,63] (RFD) in a four-component PDW (PDW4) model [44,46,47] (see also Ref. [64] for the study of a CDW model). Intuitively, RFD does nothing more than inducing the PDW short range [65]. But we will show below that in order to explain the experimental results coherently, inclusion of RFD would lead us to consider a PDW state of different nature unexplored before, thus it is not straightforward to generalize existing PDW results to our case. We consider four PDW components $\Delta_{\pm Q_{x,y}}$ at wave vectors $\pm Q_x$ and $\pm Q_y$ and all the components compete with each other. The pairing centers $\pm Q_x/2$ and $\pm Q_y/2$ are located at the intersections of the Fermi surface and the Brillouin zone boundary as shown in Fig. 1. We imagine that the PDW orders present below a characteristic temperature T^* that decreases as doping increases, as shown in Fig. 2. T^* terminates *inside* the dSC phase at a quantum critical point δ_c, which controls a quantum critical region [66–68] with special properties like linear electronic resistivity [60] (see also Ref. [61]). We first use Ginzburg-Landau (GL) formulation and Monte Carlo simulations to study the interplay of PDW, CDW and RFD in real space. A PDW with $\pm Q$ components would induce a secondary composite CDW order with wave vector $2Q$ [41,44–46], which is then coupled to the RFD [65]. With the $\pm Q$ PDW components competing with each other and the presence of RFD, it is possible to induce a TRSB loop current order compatible with the CDW. We also show that there exists a crossover temperature scale T_{CO} (see Fig. 2) for the short range static CDW order and argue that the PDW superconductivity is absent due to SC phase fluctuations. Moreover, RFD induces a domain pattern, or phase separation, on the directional PDW components at $\pm Q_x$ and $\pm Q_y$. We shall dub this state of short range PDW with four competing components the phase-separated pair nematic (PSPN) state. Next, we argue that the predominantly d-wave form factor CDW observed in STM constrains the PDW to be a bond order with $s' \pm id$-wave pairing symmetry. Using this input together with a lattice model and the GL functional, we compute the quasiparticle spectral functions under the influence of thermal fluctuations and find good agreement with ARPES.

In this study, we make several assumptions. We consider only the cuprate families that show CDW of decreasing wave vectors with increasing doping, as seen in recent x-ray scattering experiments [10,12,14]. In this study, we have neglected the cuprate families like LSCO and LBCO that show CDW wave vectors scaling with doping [38] and the CDW form factor appears to be s' wave [69], though PDW has also been suggested to play a role [40,43,44,65]. We shall focus on the experimental results in weak magnetic fields, because some recent experiments [21,22,57–59] reveal that the CDW order observed in high field and low temperature could be of a different nature than the one obtained in weak field. In the following, we neglect the dSC for simplicity and only consider the PDW order and its possible induced composite orders at a specific doping δ_0 in the phase diagram (Fig. 2). It is suggested that the d-wave superconductivity competes with the CDW [70–73]. Lastly, the origin of the PDW in cuprate is not the focus of the present paper, but some previous studies show that PDW could be originated from strong correlations [47,74].

There is another line of theory that consists of PDW as an important player. Its starting point is a spin-fluctuation scenario, captured within the spin-fermion model [75]. PDW and CDW with d-wave form factors can emerge naturally from this semimicroscopic model [76–79] (see also Ref. [80]), and it

TABLE I. Acronym list for the phrases commonly used in the paper.

Acronym	Full phrase
ARPES	Angular resolved photoemission spectroscopy
BZ	Brillouin zone
CDW	Charge density wave
dSC	d-wave SC
IUC	Intraunit cell
LC	Loop current
MC	Monte Carlo
NMR	Nuclear magnetic resonance
PDW	Pair density wave
PDW2	Two-component PDW
PDW4	Four-component PDW
PKR	Polar Kerr rotation
PND	Polarized neutron diffraction
PSPN	Phase separated pair nematic
REXS	Resonant inelastic x-ray scattering
RIXS	Resonant elastic x-ray scattering
RFD	Random field disorder
SC	Superconductor/superconductivity/superconducting
SM	Supplemental material (Ref. [98])
STM	Scanning tunneling microscopy
TRSB	Time reversal symmetry breaking

can also capture a number of important properties and features observed in the experiments. In particular, a unidirectional CDW/PDW mixed state [77,78] obtained from the model can account for the ARPES spectrum, TRSB order, CDW order, and breaking of C_4 symmetry. Although these results are similar to those of the PSPN state we discuss here, we note that in the spin-fermion model, PDW and CDW orders form a "supervector" stemming from an approximate SU(2) symmetry near the intersection points of the Fermi surface and magnetic Brillouin zone (the "hot-spots"), while here the PSPN state has the PDW as the main character and the CDW plays only a parasitic role [47,48]. As we will show below, this parasitic CDW plays a crucial part in explaining the distinct temperature scales observed in the pseudogap, namely T^* and T_{CO}. Here we wish to consider the parasitic CDW induced by the PDW only and see how far this perspective can proceed.

The paper is outlined as follow: In Sec. II, we will first briefly review the two-component PDW state, followed by the discussion of the interplay between the four-component PDW state and RFD in Sec. III. In Sec. IV, we constrain the PDW pairing symmetries from the CDW experiments. In Sec. V, we present the results for the quasiparticle spectral functions and compare with the ARPES experiments. Due to the number of acronyms, we provide an acronym list in Table I for the phrases commonly used to facilitate the reading.

II. BRIEF REVIEW ON TWO-COMPONENT PDW (PDW2)

In this section, we briefly review and discuss the model of two-component PDW (PDW2) and the effect of RFD. The main focus of the paper is to study the PDW with four components and relate to the experimental results in the pseudogap regime of the cuprates. In order to do that, it is beneficial to first discuss the PDW2 system [38,40,43–46,65], from which we can easily generalize the results to the four component case. Firstly, we will introduce the PDW order parameters consisting of two components and the corresponding GL functional. Also it is possible to induce a CDW from the PDW2, provided that both of the PDW components are nonvanishing. Next, we imagine that the CDW are coupled to the charged impurities, which are modeled by the coupling between CDW and RFD in the GL functional. For a moment, we shall consider only the subproblem of the CDW coupled to RFD, which can be cast into the random field XY model [81,82]. (Actually the random field XY model and variants have been taken as minimal models of a broad class of condensed matter systems with quenched disorders, such as flux-line arrays in dirty type-II superconductors [83], charge density waves [84], and smectic liquid crystals in random environments [85–87].) In the model, the XY phases (CDW smectic phase) are coupled to the RFD. It is found [81,82] that in 2D the RFD, no matter how weak, always induces topological defects at long scales, leading to short range (exponential) correlations in the CDW. Without disorder, the model reduces to a pure XY model, and it allows a Berezinsky-Kosterlitz-Thouless (BKT) phase transition [88,89] from a low temperature phase with power law correlation to a high temperature phase with exponential correlation. With finite RFD, the low temperature "phase" readily has exponential correlation, and the residue of the phase transition is a crossover [81], below which only short range *static* CDW order exists. Now we return to the full model containing PDW2, CDW, and RFD, which has been studied before in Ref. [65]. From the results of the random field XY model, we readily conclude that the CDW has exponential correlation. This also implies the absence of long range PDW order, since long range PDW would have induced CDW with long range correlation, contradicting the fact that the system with RFD only has short range CDW. Besides, we also expect a crossover temperature for the short range static CDW at low temperature. To this end, we will review the topological defects [45,90–92] arising in the PDW2 system (Sec. II A) and the RFD induced crossover (Sec. II B). We also present numerical evidence to show the presence of these topological defects in the PDW2 system with finite RFD in Sec. II C and lay the foundation for later numerical studies of the four-component PDW systems.

We first consider PDW2 state and its order parameter, which generally is

$$\Delta(R) = \Delta_{+Q}(R)e^{+iQ\cdot R} + \Delta_{-Q}(R)e^{-iQ\cdot R}, \tag{1}$$

where $\Delta_{\pm Q}(R) \in \mathbb{C}$. In particular, if $\Delta_{\pm Q}(R) = \Delta_0/2$ are equal and homogeneous in space, then the PDW order $\Delta(R) = \Delta_0 \cos Q \cdot R$ shows modulation of wave vector Q in real space. This state induces a CDW order at wave vector $2Q$, such that $\rho_{2Q}(R) \sim \Delta^*_{-Q}(R)\Delta_{+Q}(R)$.

In order to discuss the influence of random field disorders on the PDW and CDW state, we write down the Ginzburg-Landau (GL) functional (density) for PDW2 [46,65]:

$$F_2^\Delta = +\alpha^\Delta|\Delta|^2 + \gamma_1^\Delta|\Delta|^4 + \gamma_3^\Delta|\Delta_{+Q}|^2|\Delta_{-Q}|^2 + \kappa_\perp^\Delta|\partial_x\Delta|^2 + \kappa_\parallel^\Delta|\partial_y\Delta|^2, \tag{2}$$

where $\Delta = (\Delta_{+Q}, \Delta_{-Q})^T$. In general, the system could admit nematicity and $\kappa^{\Delta}_{\parallel,\perp}$ would differ. The other part of the GL functional involves the CDW and is given by

$$F_2^{\rho} = -H^* \rho_{2Q} + \text{c.c.} + \kappa_{\perp}^{\rho} |\partial_x \rho_{2Q}|^2 + \kappa_{\parallel}^{\rho} |\partial_y \rho_{2Q}|^2 , \quad (3)$$

where $H(R) = h_{\rm rms} h(R) e^{i\eta(R)}$ is the local complex random field, $h(R)$ are Gaussian-distributed random variables with mean 0 and standard deviation 1, $\eta(R) \in [0, 2\pi)$ are uniformly distributed random phases, and $h_{\rm rms} \geqslant 0$ controls the (root mean square) random field disorder strength. The random field term models randomly distributed nonmagnetic charged impurities that pin down the CDW modulations. Notice that the RFD couples to the CDW, which reflects the charge modulations of the PDW, but not directly to the PDW. In the following, we assume that the PDW always induces a CDW $\rho(R) \sim \rho_{2Q} \cos 2Q \cdot R$ such that

$$\rho_{2Q} = \Delta^*_{-Q} \Delta_{+Q} . \quad (4)$$

In this case, the total GL functional can be expressed in terms of $\Delta_{\pm Q}$ only as

$$\begin{aligned} F_2 &= F_2^{\Delta} + F_2^{\rho} \\ F_2^{\rho} &= -H^* \Delta^*_{-Q} \Delta_{+Q} + \text{c.c.} \\ &\quad + \kappa_{\perp}^{\rho} |\partial_x (\Delta^*_{-Q} \Delta_{+Q})|^2 + \kappa_{\parallel}^{\rho} |\partial_y (\Delta^*_{-Q} \Delta_{+Q})|^2 . \end{aligned} \quad (5)$$

We note that γ_3^{Δ} controls whether $\Delta_{\pm Q}$ components compete with each other. In this section, we shall consider $\gamma_3^{\Delta} < 0$ such that two $\Delta_{\pm Q}$ components coexist and induce a $2Q$-CDW, even in the absence of random field disorder $H(r) = 0$. The case $\gamma_3^{\Delta} > 0$ will be discussed in Sec. III.

A. Topological defects

Here we briefly discuss the possible topological defects [41,45,90,91] in the PDW2 system (in the absence of RFD). Assuming $\gamma_3^{\Delta} < 0$, then we have $|\Delta_{+Q}| \approx |\Delta_{-Q}|$. We thus write $\Delta_{\pm Q}(R) = \frac{1}{2} \Delta_0 e^{i\theta_{\pm Q}(R)}$, where we assume the amplitude fluctuations are small compared to those of the phases $\theta_{\pm Q}$. The PDW order is now

$$\Delta(R) = \Delta_0 e^{i\vartheta} \cos(Q \cdot R + \varphi) , \quad (6)$$

where the superconducting phase is $\vartheta = \frac{1}{2}(\theta_{+Q} + \theta_{-Q})$ and the PDW smectic phase is $\varphi = \frac{1}{2}(\theta_{+Q} - \theta_{-Q})$. Deep in the PDW2 phase in 2D, the amplitude fluctuations are negligible; the system can be effectively described by an anisotropic XY model in terms of the ϑ and φ [45,90–92]. The PDW2 system possesses three types of topological defects labeled by (n_v, n_d): (1) pure SC 2π-vortices with $(\pm 1, 0)$, (2) 2π-dislocations with $(0, \pm 1)$, and π-vortex-π-dislocation defect, or simply half-vortex, with $(\pm\frac{1}{2}, \pm\frac{1}{2})$. The labels (n_v, n_d) are related to the topological singularities (topological "charges") in $\vartheta(R)$ and $\varphi(R)$, defined by

$$\begin{aligned} \oint d\vec{\ell} \cdot \nabla \vartheta &= 2\pi n_v , \\ \oint d\vec{\ell} \cdot \nabla \varphi &= 2\pi n_d . \end{aligned} \quad (7)$$

Due to the single-value conditions in the original $\theta_{\pm Q}(r)$ fields, $n_{v,d}$ can take half-integer or integer values, and it leads to three types of defects in the system. Moreover, starting with a PDW2 at low temperature, owing to (thermal) proliferation of different defects, the system restores broken symmetries and yields various phases [45,91,92]. A pure CDW phase is accessed when the SC 2π vortices are proliferated and a charge-4e SC phase is obtained through the proliferation of 2π dislocations. To attain a nematic phase one needs to proliferate the half-vortices. We note that since the PDW order modulates half as many as its induced CDW, the PDW half-vortex, manifested as a 2π dislocation in the CDW, is accompanied by a half SC flux $\Phi_0/2$, which can be experimentally verified [65].

B. PDW2 with RFD

It is well known that the random field disorder destroys CDW long range order for dimension $d \leqslant 4$ [62,63]. Consider the RFD term $-H^* \Delta^*_{-Q} \Delta_{+Q} + \text{c.c.} \propto -\cos(\eta - 2\varphi)$ in Eq. (3), the CDW smectic phase 2φ tends to align with the RFD phase η. Treating the random field as a perturbation, the energy gain due to disorder potential $\sim L^{d/2}$ dominates over the elastic energy cost of adjusting to disorder $\sim L^{d-2}$. As a result, long range CDW is inhibited beyond a length scale ξ_L, known as the Larkin length. This argument implies the absence of long range PDW order if the CDW is induced by the PDW.

This picture only considers continuous elastic deformation of the uniform state, but not topological defects, which are nonperturbative in nature. Indeed, via numerical studies [81,82], it is shown that these topological defects always exist for any RFD strength in 2D. In the absence of these defects, the CDW correlation decays in power law, admitting a genuine phase transition to a high temperature phase with exponentially decaying correlation. In 2D, however, at a length scale $\xi_V > \xi_L$, the equilibrium system is always unstable to a proliferation of the static topological defects and thus the CDW correlation decays exponentially for any RFD strength.

In 2D, these CDW topological defects manifest as 2π dislocations. Retracking back to the PDW, it means a PDW half-vortex exists exactly at the CDW 2π dislocation [65]. Proliferation of these half-vortices destroys the long range PDW and lead to a nematic phase. These topological defects are pinned and static (over thermal average) at low temperature, while they can diffuse driven by thermal fluctuations at higher temperature. The presence of these defects results in short range correlations in PDW and CDW [65]. Instead of a genuine phase transition, we thus expect a crossover temperature T_{CO}, below which short range static charge order can be observed, and above which most of the charge order is destroyed by the defect diffusion (except domains that are pinned strongly by the RFD). Here only an argument is given; we shall provide numerical evidence in Sec. III.

C. Numerics: Monte Carlo study of PDW2 with RFD

In order to gain more intuition on the interplay of PDW, CDW and RFD in a PDW2 system, we perform Monte Carlo study on the corresponding lattice GL functional [65],

$$F_{2,\text{lattice}} = F^{\Delta}_{2,\text{lattice}} + F^{\rho}_{2,\text{lattice}} \quad (8)$$

with

$$F^{\Delta}_{2,\text{lattice}} = +\tilde{\alpha}^{\Delta}\sum_{\mathbf{i}s}|\Delta_{sQ}(\mathbf{i})|^2 + \gamma_1^{\Delta}\sum_{\mathbf{i}}\left(\sum_{s}|\Delta_{sQ}(\mathbf{i})|^2\right)^2 + \gamma_3^{\Delta}\sum_{\mathbf{i}}|\Delta_{+Q}(\mathbf{i})|^2|\Delta_{-Q}(\mathbf{i})|^2$$
$$- 2\kappa_{\perp}^{\Delta}\sum_{\mathbf{i}s}\text{Re}[\Delta_{sQ}(\mathbf{i}+\hat{x})\Delta^{*}_{sQ}(\mathbf{i})] - 2\kappa_{\parallel}^{\Delta}\sum_{\mathbf{i}s}\text{Re}[\Delta_{sQ}(\mathbf{i}+\hat{y})\Delta^{*}_{sQ}(\mathbf{i})]$$

$$F^{\rho}_{2,\text{lattice}} = -2h_{\text{rms}}\sum_{\mathbf{i}}\text{Re}[h(\mathbf{i})e^{-i\eta(\mathbf{i})}\Delta^{*}_{-Q}(\mathbf{i})\Delta_{+Q}(\mathbf{i})] - 2\kappa_{\perp}^{\rho}\sum_{\mathbf{i}}\text{Re}[\Delta_{-Q}(\mathbf{i}+\hat{x})\Delta^{*}_{+Q}(\mathbf{i}+\hat{x})\Delta^{*}_{-Q}(\mathbf{i})\Delta_{+Q}(\mathbf{i})]$$
$$- 2\kappa_{\parallel}^{\rho}\sum_{\mathbf{i}}\text{Re}[\Delta_{-Q}(\mathbf{i}+\hat{y})\Delta^{*}_{+Q}(\mathbf{i}+\hat{y})\Delta^{*}_{-Q}(\mathbf{i})\Delta_{+Q}(\mathbf{i})] + 2(\kappa_{\parallel}^{\rho}+\kappa_{\perp}^{\rho})\sum_{\mathbf{i}}|\Delta_{-Q}(\mathbf{i})\Delta_{+Q}(\mathbf{i})|^2$$

on a square lattice. Here $\tilde{\alpha}^{\Delta} = \alpha^{\Delta} + 2\kappa_{\parallel}^{\Delta} + 2\kappa_{\perp}^{\Delta}$ and the summation is over site $\mathbf{i}$ and sign $s = \pm$. $\hat{x}$ and $\hat{y}$ are shifts by one lattice constant in the corresponding directions in real space. The random fields $h(\mathbf{i})e^{i\eta(\mathbf{i})}$ are Gaussian distributed at each site. If we choose $\gamma_3^{\Delta} < 0$, we can safely set the amplitudes $|\Delta_{\pm Q}|$ as constants for the system at low enough temperature and only be concerned about the phase fields $\theta_{\pm Q}(\mathbf{i})$. This essentially reduces to a random field XY model [65], on which we perform the Monte Carlo (MC) simulations with Metropolis algorithm of single-site phase rotations. The initial PDW phases $\theta_{\pm Q}$ are initialized randomly at a high enough temperature, which is then slowly lowered to the desired one. This simulated annealing process lets the system be better equilibrated at the final temperature. At the final temperature, we measure the thermal averaged phases of $\Delta_{\pm Q}$ and $\rho_{2Q} = \Delta^{*}_{-Q}\Delta_{+Q}$ at each site. For simplicity, we choose $\kappa_{\parallel} = \kappa_{\perp}$.

In Fig. 3, the results are shown for a typical RFD configuration. Due to their single-value conditions, we show the $\theta_{\pm Q}$ fields instead of the ϑ and φ fields. The choice of parameters deserves some comments. Restricting to $\gamma_3^{\Delta} < 0$ (i.e., coexisting $\Delta_{\pm Q}$), the phase diagram for $F_{2,\text{lattice}}$ turns out to be simple. In Ref. [65] it is found that there are only two phases: the fully disordered phase with the presence of all types of topological defects and the PDW glass phase, in which no CDW dislocation of 2π winding is allowed (only 4π defects are permitted). The parameters in Fig. 3 correspond to the fully disordered phase due to the presence of 2π defects. The PDW glass phase is interesting in its own right, but we shall only consider the fully disordered phase here. Back to Fig. 3, several observations are in order. First, the CDW phase $2\varphi(\mathbf{i})$ forms "domains." This is consistent with our previous discussion that a few sites bare strong random fields and the CDW phases near these sites would align along with these strong random fields under the influence of the stiffness terms $\kappa^{\Delta,\rho}$. Next is the existence of 2π dislocations (2π windings) in the CDW phase [Figs. 3(c) and 3(d)]. We note that these defects occur near the domain boundary since by doing so the system can lower its energy better than pure continuous elastic deformation [81]. These dislocations come in pairs of opposite windings, which is expected in the system with periodic boundary condition and zero total winding.

We note that this simulated method can be utilized to find the ground state of the system, but what we have found might not be the true ground state and it is not our main object to do so. Indeed, the system shows glassy behavior that it can be trapped in some local energy minimum. This can be understood in terms of the phase relation $2\varphi = \theta_{+Q} - \theta_{-Q}$ that although the CDW dislocations are largely determined by the RFD configuration, a CDW 2π dislocation can manifest itself as a 2π vortex in either PDW component $\Delta_{\pm Q}$ [see Figs. 3(a) and 3(b)]. This "selection" depends on the initial configurations and the simulated annealing process (for instance, the temperature intervals during cooling and the MC steps for each temperature). Different selection would give a

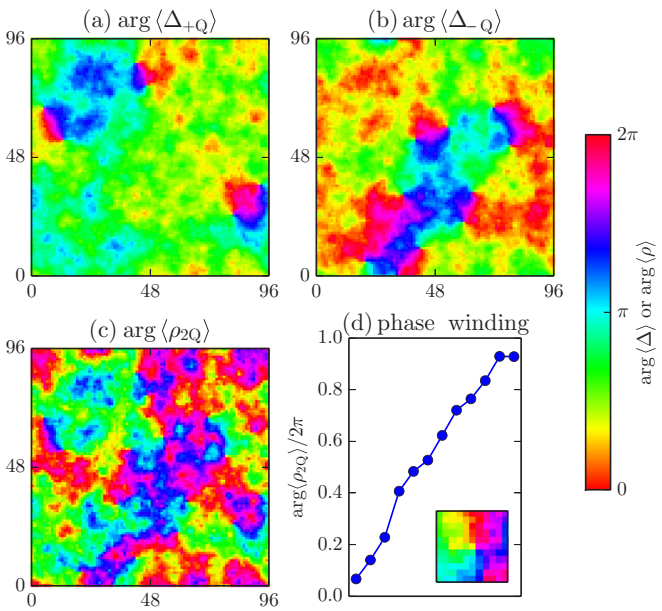

FIG. 3. Monte Carlo results for PDW2 system in $F_{2,\text{lattice}}$ [Eq. (8)]. The phases of the average orders (a) $\langle\Delta_{+Q}\rangle$, (b) $\langle\Delta_{-Q}\rangle$, and (c) $\langle\rho_{2Q}\rangle$ are shown. Here we choose $\gamma_3^{\Delta} < 0$ such that we can consider the phases and their fluctuations only and assume constant order magnitudes. In (a) and (b), several defect pairs with opposite windings are present in $\langle\Delta_{\pm Q}\rangle$. Due to the fact that the CDW is induced by the PDW, these defect pairs also manifest in the $\langle\rho_{2Q}\rangle$ [see (c)]. As an example, panel (d) shows a 2π CDW smectic phase winding around a counterclockwise path of a CDW 2π dislocation (see the inset) located near $\vec{R} = (53,60)$. Parameters (in meV): $\kappa_{\parallel,\perp}^{\Delta} = 5$, $\kappa_{\parallel,\perp}^{\rho} = 1$, $h_{\text{rms}} = 4$, $\alpha^{\Delta}, \gamma_3^{\Delta} < 0$, and $\gamma_1^{\Delta} > 0$. System size: 96×96 with periodic boundary condition. Simulated annealing is performed from a high temperature to the final temperature at 10 K.

slightly different total energy, but it is understood that in 2D, the interplay of PDW, CDW, and RFD always produces a short range PDW and CDW state with the presence of topological defects.

III. PHASE-SEPARATED PAIR NEMATIC (PSPN) STATE

In this section, motivated by the STM and REXS experimental results, we introduce a four-component PDW (PDW4) state with phase separation in directional components, which is dubbed as a phase-separated pair nematic (PSPN) state. Experimentally, STM results [19,56] reveal that the presence of short range CDW within the pseudogap regime. These CDW orders are directional and have wave vectors $2Q_x$ and $2Q_y$. It is also shown that these two CDW components compete with each other in real space and form a domain structure, or phase separation pattern. This picture is also supported by the REXS [13] showing that the results are more consistent with stripy CDW domains. Viewing this in terms of PDW (Section II), within each domain, the directional CDW with $2Q_a$ ($a = x,y$) is actually induced by a PDW2 with components $\Delta_{\pm Q_a}$, and this subsystem can be described by the PDW2 model Eq. (8). However, for the global system with Δ_x and Δ_y domains (Δ_a denotes $\Delta_{\pm Q_a}$ components), we have to generalize to a PDW4 model [40,41,43–48]. Moreover, in order to reproduce the phase separation pattern, we shall consider strong competition in the directional components Δ_a [$\gamma_2^\Delta > 0$, see Eq. (10) below].

On the other hand, TRSB order is detected in the pseudogap by PKR [25,54] and PND [27–29]. The experiments seem to support that the loop current (LC) order [49] is responsible for the TRSB order. A natural question would be whether we can explain this TRSB order within the PDW4 model. Interestingly, Agterberg *et al.* [48] proposed that the LC order can arise from a PDW theory as a secondary composite order. However, it is readily discovered that within the PDW4 model the LC order is incompatible with the induced CDW in a PDW state with spatially homogeneous components Δ_Q. One way to resolve this issue is to introduce an eight-component PDW model, as done by Agterberg *et al.* [48], while another feasible way, as will be demonstrated below, is to include RFD and to relax the assumption that the state has homogeneous PDW components.

In the PDW4 model, another relevant parameter is γ_3^Δ [see Eq. (10) below] controlling whether the Δ_{+Q_a} and Δ_{-Q_a} components compete. If the components $\Delta_{\pm Q_a}$ are assumed to be spatially independent, from the known results on the possible PDW4 ground states [41,48], we are constrained to choose $\gamma_3^\Delta < 0$ such that Δ_{+Q_a} and Δ_{-Q_a} can coexist. Otherwise, no CDW $\rho_{2Q_a} = \Delta^*_{-Q_a}\Delta_{+Q_a}$ can be induced, contradicting the experimental results discussed above. By introducing disorders in the form of RFD, we break the translational invariance and allow the PDW components $\Delta_{\pm Q_a}$ to be spatially inhomogeneous. We will demonstrate that in this setting, the parameter range $\gamma_3^\Delta > 0$ (for competing Δ_{+Q_a} and Δ_{-Q_a}) should also be taken into account. Inclusion of RFD and the parameter choice of $\gamma_2^\Delta, \gamma_3^\Delta > 0$ lead to two important consequences: (i) generating a phase separation in $\rho_{2Q_{x,y}}$ (induced by $\Delta_{x,y}$) that is consistent with that observed in the experiments and (ii) resolving the incompatibility issue of CDW and LC orders within the PDW4 model. Furthermore, we show that in the PDW4 model there is also a crossover temperature $T_{CO} < T^*$ to account for the short range static CDW within the pseudogap. For temperature $T_{CO} < T < T^*$, the induced CDW is dynamically fluctuating. The simulation result also suggests that the PDW superconductivity is absent owing to strong SC phase fluctuations, complying with nonsuperconducting pseudogap. These results constitute the properties of the PSPN state.

We consider the PDW4 system on a square lattice. We shall assume that the two new components $\Delta_{\pm Q_x}$ are related to the PDW2 components $\Delta_{\pm Q}$ with $Q = Q_y$ by a $\pi/2$ rotation. By construction, we require that $Q_x \neq Q_y$. The order parameter is given by

$$\Delta(\mathbf{i}) = \sum_{as} \Delta_{sQ_a}(\mathbf{i}) e^{isQ_a\cdot x_\mathbf{i}}. \tag{9}$$

We write down the lattice PDW4 GL functional [46] by generalizing the PDW2 case,

$$F_{4,\text{lattice}} = F^\Delta_{4,\text{lattice}} + F^\rho_{4,\text{lattice}} \tag{10}$$

with

$$\begin{aligned}
F^\Delta_{4,\text{lattice}} =& -2\kappa^\Delta_\parallel \sum_{\mathbf{i}as} \text{Re}\left[\Delta_{sQ_a}(\mathbf{i}+a_\parallel)\Delta^*_{sQ_a}(\mathbf{i})\right] - 2\kappa^\Delta_\perp \sum_{\mathbf{i}as} \text{Re}\left[\Delta_{sQ_a}(\mathbf{i}+a_\perp)\Delta^*_{sQ_a}(\mathbf{i})\right] \\
&+ \tilde{\alpha}^\Delta \sum_{\mathbf{i}as} \left|\Delta_{sQ_a}(\mathbf{i})\right|^2 + \gamma_1^\Delta \sum_{\mathbf{i}} \left(\sum_{as} \left|\Delta_{sQ_a}(\mathbf{i})\right|^2\right)^2 + \gamma_2^\Delta \sum_{\mathbf{i}} \left(\sum_{s} \left|\Delta_{sQ_x}(\mathbf{i})\right|^2\right)\left(\sum_{s} \left|\Delta_{sQ_y}(\mathbf{i})\right|^2\right) \\
&+ \gamma_3^\Delta \sum_{\mathbf{i}a} \left|\Delta_{+Q_a}(\mathbf{i})\right|^2 \left|\Delta_{-Q_a}(\mathbf{i})\right|^2 + 2\gamma_4^\Delta \sum_{\mathbf{i}} \text{Re}\left[\Delta_{+Q_x}(\mathbf{i})\Delta_{-Q_x}(\mathbf{i})\Delta^*_{+Q_y}(\mathbf{i})\Delta^*_{-Q_y}(\mathbf{i})\right] \\
F^\rho_{4,\text{lattice}} =& -2h_{\text{rms}} \sum_{\mathbf{i}a} \text{Re}\left[h_a(i)e^{-i\eta_a(\mathbf{i})}\Delta^*_{-Q_a}(\mathbf{i})\Delta_{Q_a}(\mathbf{i})\right] - 2\kappa^\rho_\parallel \sum_{\mathbf{i}a} \text{Re}\left[\Delta_{-Q_a}\cdot\Delta^*_{+Q_a}(\mathbf{i}+a_\parallel)\Delta^*_{-Q_a}\cdot\Delta_{+Q_a}(\mathbf{i})\right] \\
&- 2\kappa^\rho_\perp \sum_{\mathbf{i}a} \text{Re}\left[\Delta_{-Q_a}\cdot\Delta^*_{+Q_a}(\mathbf{i}+a_\perp)\Delta^*_{-Q_a}\cdot\Delta_{+Q_a}(\mathbf{i})\right] + 2(\kappa^\rho_\parallel + \kappa^\rho_\perp) \sum_{\mathbf{i}a} \left|\Delta_{-Q_a}(\mathbf{i})\Delta_{+Q_a}(\mathbf{i})\right|^2,
\end{aligned}$$

where we have implicitly replaced $\rho_{2Q_a} \to \Delta^*_{-Q_a}\Delta_{+Q_a}$ and $\Delta^*_{-Q_a}\cdot\Delta_{+Q_a}(\mathbf{i})$ denotes $\Delta^*_{-Q_a}(\mathbf{i})\Delta_{+Q_a}(\mathbf{i})$ for brevity. Here the summation is over $a = x, y$, and $\tilde{\alpha}^\Delta = \alpha^\Delta + 2\kappa^\Delta_\parallel + 2\kappa^\Delta_\perp$. The notation $a_\parallel = a$ and $a_\perp = \hat{y}\,(\hat{x})$ if $a = \hat{x}\,(\hat{y})$. The rest is similar as in the PDW2 case, except that now we have four PDW components at $\pm Q_{x,y}$ and allow coupling (γ_2^Δ term) between the directional components. Notice that each $2Q_a$-CDW is coupled to a different random field disorder $h_a e^{i\eta_a}$.

In the absence of RFD $h_{\rm rms} = 0$, the ground state of the PDW4 functional is mainly controlled by γ_2 and γ_3. As in the PDW2 case, the sign of γ_3^Δ controls whether two components Δ_{+Q_a} and Δ_{-Q_a} ($a = x, y$) coexist ($\gamma_3^\Delta < 0$) or compete ($\gamma_3^\Delta > 0$) with each other. While the sign of γ_2^Δ dictates the coexistence ($\gamma_2^\Delta < 0$) or competition ($\gamma_2^\Delta > 0$) of $|\Delta_x|^2$ and $|\Delta_y|^2$ components, where $|\Delta_a|^2 = \sum_s |\Delta_{sQ_a}|^2$. In the literature, the main concern is on the latter. (There is also a similar debate [93,94] on the pure CDW model.) In Refs. [43–45], the authors propose a PDW theory with $\gamma_2^\Delta > 0$ and $\gamma_3^\Delta < 0$ such that in a clean 2D system, the ground state is a (unidirectional) striped PDW with either Δ_x or Δ_y component. On the other hand, Ref. [47] suggests a bidirectional PDW state with $\gamma_2^\Delta, \gamma_3^\Delta < 0$ that the $\Delta_{x,y}$ components coexist. Experimentally, x-ray scattering measurements [13,15] reveal the CDW with only wave vectors $2Q_x$ and $2Q_y$ but not $\pm 2Q_x \pm 2Q_y$. If the PDW, as well as the induced CDW, is bidirectional, then it is likely that the $\pm 2Q_x \pm 2Q_y$ CDW components would be observed [93] (see, however, Ref. [47]). Here we propose another parameter choice $\gamma_2^\Delta, \gamma_3^\Delta > 0$ such that all four components Δ_{sQ_a} compete with each other and constitute the PSPN state. We shall show that it can generate, besides the CDW orders, a LC order [49] accounting for the polar Kerr effect and the intraunit cell time-reversal symmetry breaking order observed respectively in the PKR and PND experiments.

The (phenomenological) LC order emerged from PDW order $\Delta_{\pm Q_a}$ is defined as [48]

$$l_a = \left|\Delta_{+Q_a}\right|^2 - \left|\Delta_{-Q_a}\right|^2. \tag{11}$$

This order parameter is translational invariant (hence giving rise to an IUC order observed in PND), odd under either time reversal symmetry and parity, and invariant under their product. (We note that from a pure CDW order, one can also construct a similar composite TRSB order [95,96]) Since this LC order is originated from the PDW, its characteristic temperature is the same as T^*, which is indeed observed in the PND [27–29]. At first sight, in the PDW4 model this order l_a is incompatible with the CDW order ρ_{2Q_a}. If we restrict ourselves to spatially independent order, then a finite l_a would require $\gamma_3^\Delta < 0$, which leads to one of the Δ_{+Q_a} and Δ_{-Q_a} components to vanish, and eventually the induced CDW order $\rho_{2Q_a} = 0$. This is the reason why the authors in Ref. [48] turn to an eight-component PDW theory. For details of the eight-component theory, the readers shall refer to the reference. Here we will demonstrate that if we relax the assumption of spatial homogeneity of the order parameters and introduce RFD, finite orders in both l_a and ρ_{2Q_a} are actually compatible within the PDW4 model.

Before diving into the numerics, we shall first consider a simplified model to understand the interplay of (short range)

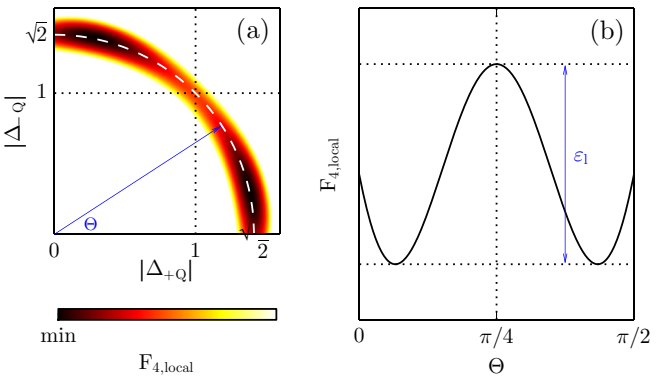

FIG. 4. (a) Schematic density plot of $F_{4,\rm local}$ [Eq. (12)] as a function of $|\Delta_{\pm Q}|$ for $\gamma_3^\Delta > h_{\rm rms} > 0$. (b) Plot of $F_{4,\rm local}$ as a function of Θ defined in (a) along the white dashed line with $\sum_s |\Delta_{sQ}|^2 = -\frac{\alpha^\Delta}{2\gamma_1^\Delta} = 2$. $F_{4,\rm local}$ has two minima separated by an energy barrier ε_l. At either minimum, the induced CDW ρ_{2Q} and LC order l are both finite.

CDW and LC order with the RFD. The simplified "on-site" model is given by

$$F_{4,\rm local} = +\alpha^\Delta \sum_s |\Delta_{sQ}|^2 + \gamma_1^\Delta \left(\sum_s |\Delta_{sQ}|^2\right)^2 + \gamma_3^\Delta |\Delta_{+Q}|^2 |\Delta_{-Q}|^2 - 2h_{\rm rms}|\Delta_{-Q}\Delta_{+Q}| \tag{12}$$

such that we can ignore the phase degrees of freedom. Here we have already assumed $\gamma_2^\Delta > 0$ and only one pair of $\Delta_{\pm Q}$ exists locally. We further assume that the CDW smectic phase is already aligned with the local pinning field such that the RFD term reduces to the present form. Now we notice that although $\gamma_3^\Delta > 0$ would suppress one of the $\Delta_{\pm Q}$ components, but the RFD term ($h_{\rm rms} > 0$) induces a finite CDW order $\sim|\Delta_{-Q}\Delta_{+Q}|$ such that both $\Delta_{\pm Q} \neq 0$. This competition, provided with the suitable parameters (see Fig. 4), can result in a local state with both nonvanishing ρ_{2Q} and l. We shall briefly remark that the effect of RFD on the eight-component PDW theory [48], in which the incompatibility issue of CDW and LC order is solved by introducing extra competing PDW components. If RFD is introduced, then using a similar argument as above, it is likely that extra CDW components other than those of wave vectors $2Q_x$ and $2Q_y$ can be induced. While currently there is no experimental evidence showing these extra CDW components. On the other hand, in Fig. 4 we notice an interesting feature that the two minima are separated by an energy barrier ε_l. One may define a temperature scale $T_K \sim \langle\varepsilon_l(\mathbf{i})\rangle_\mathbf{i}$ as the spatial average of the energy barriers, which characterizes the stiffness of the state to (thermally activated) relative amplitude fluctuations between $|\Delta_{+Q_a}|$ and $|\Delta_{-Q_a}|$. For $T < T_K$, the energy barrier hinders the relative amplitude fluctuations, and this results in finite LC order. For $T > T_K$, the thermal fluctuations overcome the energy barriers and the system now consists of fluctuating LC order domains with different signs leading to a thermal average $\langle\sum_a l_a\rangle \sim 0$ for TRSB order. This argument might explain the disparity between the temperature scales for TRSB order measured in PKR and PND, in which the one measured

in PKR is strictly lower than that in PND (see Introduction). The elaborated study however will be pursued elsewhere.

Now back to the entire system described by $F_{4,\text{lattice}}$ [Eq. 10] with RFD $h_{\text{rms}}h(R)e^{i\eta(R)}$, we focus on those sites with particularly strong pinning strengths. At one of these sites, to gain the pinning energy, the CDW smectic phase would align with the RFD phase η (see Sec. II B). The PDW and CDW stiffness terms would induce a finite region of approximately the same smectic phase around the strong disorder site. Now if we are restricted to the parameter choice discussed above and take the directional PDW into account, we would then expect a phase separated domain pattern, in which the directional PDW, together with the induced directional CDW and LC orders, presents due to the "nucleation" around these strong disorders. The phase separated orders discussed above can be regarded as imposing phase separation patterns on the PDW2 orders. This indicates that the correlations of the PDW and CDW orders are bounded by those in PDW2, and thus the resultant state also has PDW and CDW with the short range exponential correlations. Analog to the PDW2 case, we also expect a crossover temperature for the short range static CDW in the state. Owing to the phase separation pattern and the local nematicity originated from PDW superconductivity, we shall call this the phase-separated pair nematic (PSPN) state. Below we will demonstrate that the PSPN state can result from the PDW4 GL functional with RFD [Eq. (10)] via MC simulation study.

A. Numerics: Monte Carlo study of PSPN

To better illustrate our points, we perform the MC simulations similar to the PDW2 case. We consider the case of $\gamma_{2,3}^{\Delta} > 0$ as we discussed above and choose α^{Δ} and γ_1^{Δ} such that the average $|\Delta_{sQ_a}| \sim 1$. We divide the MC study into two stages. In the first stage, in order to capture the effects of $\gamma_{2,3}^{\Delta}$ on the resultant state, we allow updates (Metropolis algorithm, single site) on both the amplitudes and phases of the PDW order parameters. We start with a random phase configuration with $|\Delta_{sQ_a}| = 1$ and perform the simulated annealing process to let the system better equilibrate at the final temperature. For later comparison to experimental data, the simulation is performed with a typical RFD configuration. We then obtain a state at low temperature, resembling the ground state for a given set of parameters. In the second stage, we are interested in the effect of thermal fluctuations on the orders, in particular the phase fluctuations induced by proliferation of topological defects (see Sec. II A). Analog to the studies of BKT transition [88,89] (see also random field XY model [65,81]), we shall assume that the system is deep in the state obtained in stage one. We thus utilize the averaged amplitudes as input (i.e., the amplitudes are kept fixed during the MC) and only perform MC simulations with phase updates (Metropolis algorithm, single site) for various temperatures. To be consistent, α^{Δ} and γ_1^{Δ} used in stage one should be chosen to suppress the the total PDW amplitude fluctuations but still permit sufficient acceptance rates for sampling states with various relative PDW amplitudes. Besides, directional CDW with wave vectors $2Q_{x,y}$ requires that γ_2^{Δ} is dominated over γ_3^{Δ}, while in order to induce finite orders in both CDW and LC order, γ_3^{Δ} and h_{rms} should be comparable (see Fig. 4). We shall set $\gamma_4^{\Delta} = 0$ such that the phases of the directional PDW are not coupled [97].

In Fig. 5, we show the simulation results in stage one for a typical RFD configuration for PDW4. Several observations are followed. Owing to a large $\gamma_2^{\Delta} > 0$, the two components $\Delta_{x,y}$ compete with each other, and it results in phase separation for $\Delta_{x,y}$, as well as $\rho_{2Q_{x,y}}$. (Recall that Δ_a denotes directional PDW components $\Delta_{\pm Q_a}$) Within each domain of $\Delta_{x,y}$ and $\rho_{2Q_{x,y}}$, the phases (arg $\Delta_{\pm Q_a}$ and arg ρ_{2Q_a}) have similar domain structures as in the PDW2 case, except that there are regions of vanishing amplitude in which the phases are not well defined. There are still topological defects in the domains, but the number is not well constrained due to the regions of vanishing amplitude. Experimentally, CDW dislocations of 2π windings are indeed observed in STM [19], and they could trap the half SC fluxes for a PDW state (see Sec. II A), provided that the SC phase is strongly pinned. One can probe these half fluxes by SQUID microscopy and test the proposed PDW theory. Next, we notice both ρ_{2Q_a} and l_a have finite magnitude locally, in accord with our discussion on the simplified model Eq. (12). Also, as discussed, the PDW and CDW orders are expected to be short ranged and decay exponentially [65,81] (see Fig. 1 in the Supplemental Material [98] (SM) for numerical evidence and more discussions), due to the random phases and the presence of topological defects. The LC order l_a are inhomogeneous and have random signs. This selection of the local sign is related to the initial configuration and simulated annealing process. We also note that the amplitudes $|\Delta_{sQ_a}|$ are inhomogeneous, to accommodate both nonvanishing ρ_{2Q_a} and l_a. Again, the simulation might be trapped at some local energy minimum and unable to attain the true ground state, but the main purpose is to illustrate the effect of RFD and the simultaneous presence of l_a and ρ_{2Q_a} for our choice of $\gamma_3^{\Delta} > 0$.

We then move on to stage two to study the effect of the thermal phase fluctuations on the PDW and CDW orders. As discussed, owing to the pinning of the RFD, the PDW and CDW orders are short ranged, and we expect a crossover temperature T_{CO} for the static CDW. To determine T_{CO}, we plot the temperature dependent *local* CDW order $\bar{\rho}^{\text{local}}$, as well as local order $\bar{\Delta}^{\text{local}}$ for PDW, in Fig. 6. The local orders decay in a continuous fashion as temperature increases. At low temperature, the local charge orders with significant amplitude are still present, as shown in Fig. 7(a), due to the strong pinning effect of the RFD and correlation effect of the stiffness terms $\kappa^{\Delta,\rho}$. At high enough temperature, the local charge orders are almost absent [Fig. 7(b)], as the thermal phase fluctuations have overcome the pinning effect from RFD and stiffness terms. We can view this as the thermally activated diffusion of the topological defects (dislocations) of the CDW. Moreover, although the amplitudes are kept fixed as the averaged values taken from Fig. 5, we notice that as a manifestation of the strong phase fluctuations, the domains of well-defined CDW smectic phase at high temperature [Fig. 7(b)] shrink considerably. We shall roughly identify the crossover temperature for the short range static CDW $T_{CO} = 150\,\text{K}$ by setting the threshold $\rho_0 = 0.2$ [99]. In this sense, Figs. 7(a) and 7(b) actually correspond to the spatial variations of the directional CDW for $T < T_{CO}$ and $T > T_{CO}$, respectively.

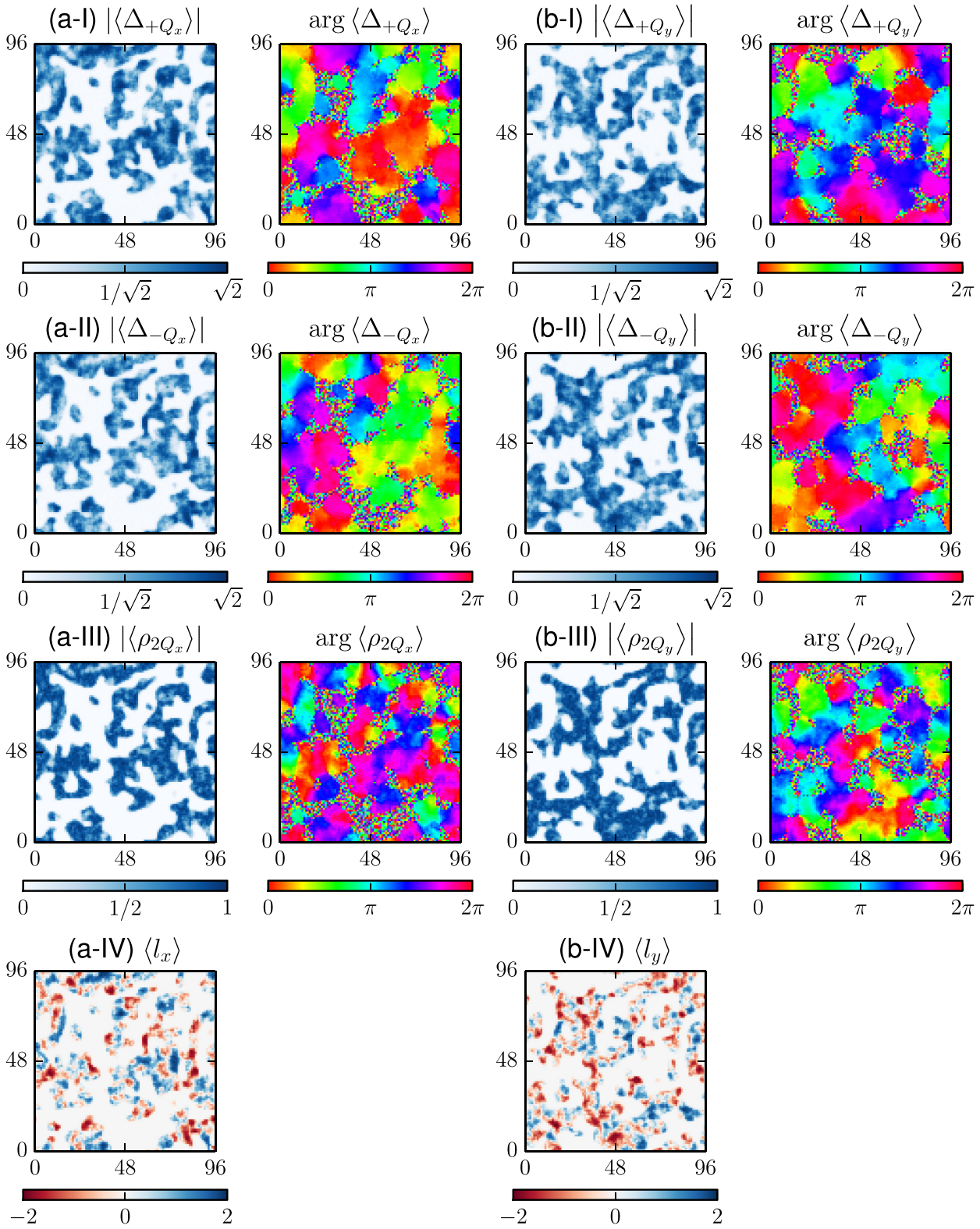

FIG. 5. Monte Carlo results of the PSPN state in the presence of RFD for the averaged order parameters in (a) x- and (b) y-directions, using GL functional $F_{4,\text{lattice}}$ Eq. (10). We plot the spatial dependent (I and II) PDW components $\langle\Delta_{\pm Q_a}\rangle$, (III) CDW $\langle\rho_{2Q_a}\rangle$ and (IV) LC order $\langle l_a\rangle$. The PDW and CDW orders are phase separated in the directional components. Also the PDW and CDW phases $\arg\langle\Delta_{sQ_a}\rangle$ and $\arg\langle\rho_{2Q_a}\rangle$ form a domain pattern, similar to the PDW2 case. Moreover, finite CDW and LC orders are induced in the system. In order to capture the effects of $\gamma^{\Delta}_{2,3} > 0$, we allow updates on both amplitudes and phases of the PDW order parameters Δ_{sQ_a}. Parameters (in meV): $\alpha^{\Delta} = -100$, $\gamma^{\Delta}_1 = 25$, $\gamma^{\Delta}_2 = 20$, $\gamma^{\Delta}_3 = 5$, $\gamma^{\Delta}_4 = 0$, $\kappa^{\Delta}_{\parallel,\perp} = 10$, $\kappa^{\rho}_{\parallel,\perp} = 1$, $h_{\text{rms}} = 2$. System size: 96×96 with periodic boundary condition. Simulated annealing is performed from a high temperature to the final temperature at 10 K.

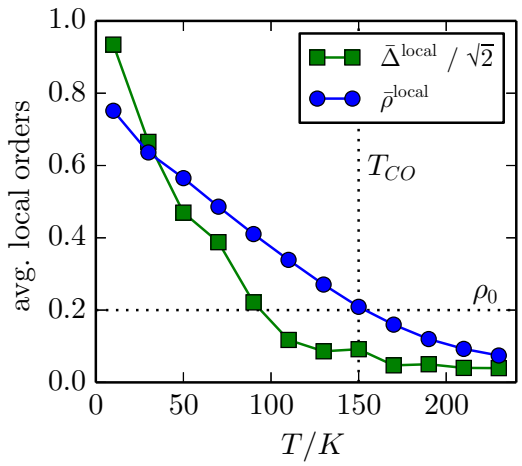

FIG. 6. Melting of short range PDW and CDW in the PSPN state in the presence of RFD by performing MC simulations on GL functional $F_{4,\rm lattice}$ [Eq. (10)]. As a function of temperature, the averaged *local* PDW and CDW orders, defined as $\bar{\Delta}^{\rm local} = \frac{1}{N}\sum_{\mathbf{i}}\sqrt{\sum_{sa}|\Delta_{sQ_a}(\mathbf{i})|^2}$ and $\bar{\rho}^{\rm local} = \frac{1}{N}\sum_{\mathbf{i}a}|\rho_{2Q_a}(\mathbf{i})|$, are plotted, where N is the total number of sites. Notice that the plotted values are rescaled by their maximal possible values. In order to study the effect of the phase fluctuations, the amplitudes of the PDW components $|\Delta_{sQ_a}|$ are taken from the averaged results in Fig. 5 as input and kept constant during the simulations, while only the phases $\arg\Delta_{sQ_a}$ are updated. We set the threshold $\rho_0 = 0.2$ [97] for the local CDW order to define the crossover temperature T_{CO} for the short range static CDW orders. Parameters are the same as in Fig. 5.

Next we discuss whether the PDW superconductivity can survive the thermal phase fluctuations. Figure 8 shows the MC results for the magnitudes and phases of the averaged PDW orders $\langle\Delta_{sQ_a}\rangle$ at $T = 50\,\mathrm{K}$ and 190 K. At $T = 50\,\mathrm{K} < T_{CO}$ [Fig. 8(a)], there are PDW domains with almost vanishing amplitudes, in contrast to the same area in Fig. 7(a), in which charge orders of significant amplitude still remain. This difference is because of the strong pinning on the CDW smectic phase by the RFD, while PDW superconducting phases $\vartheta_a \equiv \frac{1}{2}(\theta_{+Q_a} + \theta_{-Q_a})$ are not (here $\theta_{sQ_a} \equiv \arg\Delta_{sQ_a}$ are the phase fields of the PDW components, see also Sec. II A). Since the PDW smectic phases $\varphi_a \equiv \frac{1}{2}(\theta_{+Q_a} - \theta_{-Q_a})$ are also pinned indirectly by the RFD through the induced CDW below T_{CO}, this suggests that the fluctuations in the SC phases ϑ_a in the domains are strong. We note that the phase fluctuations are stronger than the PDW2 case due to the phase separation pattern [97]. The thermal fluctuations can "invade" the orders at the boundaries and destroy them more severely than the system without phase separation. At $T = 190\,\mathrm{K} > T_{CO}$ [Fig. 8(b)], the thermal fluctuations are severe and the PDW local order is mostly wiped out, as evident from the vanishing averaged PDW order parameters and the considerable shrinkage in the PDW domains of well-defined phases. It is well known that dynamic vortices in a superconductor dissipate supercurrent, leading to a finite resistance (known as the *flux flow resistance*, see, e.g., Ref. [100]). In this regard, the results in Fig. 8 hint that the PDW superconductivity is absent owing to strong thermal fluctuations in the superconducting phase irrespective of the crossover temperature T_{CO} and appear to be consistent with the known fact that the pseudogap is nonsuperconducting.

We conclude this section by comparing these results with experiments. First, RIXS [8,9,11] and STM [17] reveal traces of the crossover temperature T_{CO} for static charge order inside the pseudogap. RIXS uses hard x-rays to measure the static order of a given structure. Similarly STM measures the static electronic orders. T_{CO}'s found in these probes show a similar trend that is peaked at some doping. Comparing with our results, we identify the order to be the short range CDW. REXS measurements however use soft x-rays, that are sensitive to fluctuating orders, and they can detect the fluctuating CDW up to a higher temperature T^*, at which the PDW orders vanish. Next, a smectic modulation measure $O_s^Q(r,e)$ in STM [18,19,56] signifies relative strength of the local smectic (directional) electronic orders. As discussed at

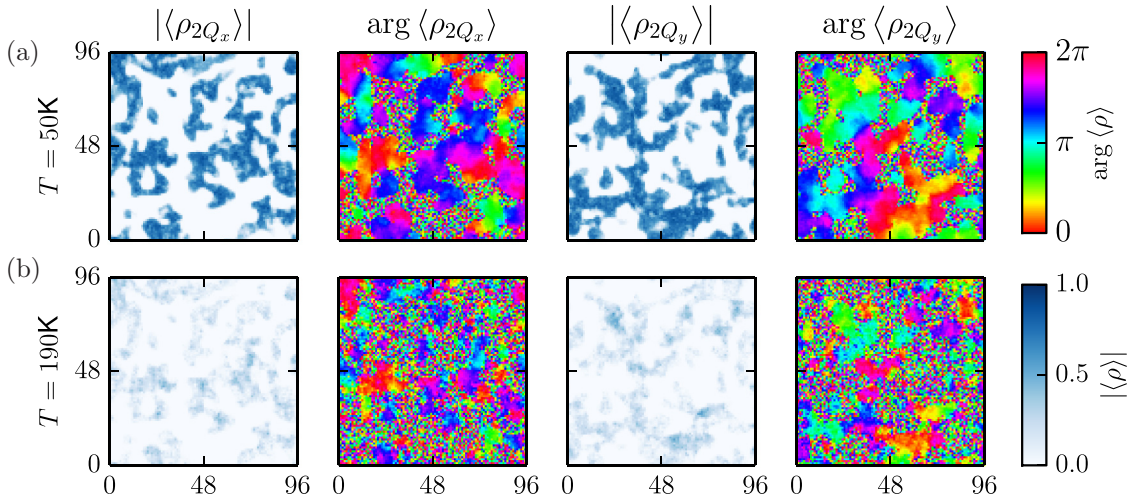

FIG. 7. Spatial variations of CDW in the PSPN state at two temperatures: (a) $T = 50\,\mathrm{K} < T_{CO}$ and (b) $T = 190\,\mathrm{K} > T_{CO}$. In the same MC simulations of Fig. 6 using GL functional $F_{4,\rm lattice}$ [Eq. (10)], we show the results for the averaged directional CDW $\langle\rho_{2Q_a}\rangle$. The noticeable difference for these two temperatures is the vanishing small magnitudes of the averaged CDW at $T = 190\,\mathrm{K}$ due to the strong thermal fluctuations in the smectic phases for $T > T_{CO}$.

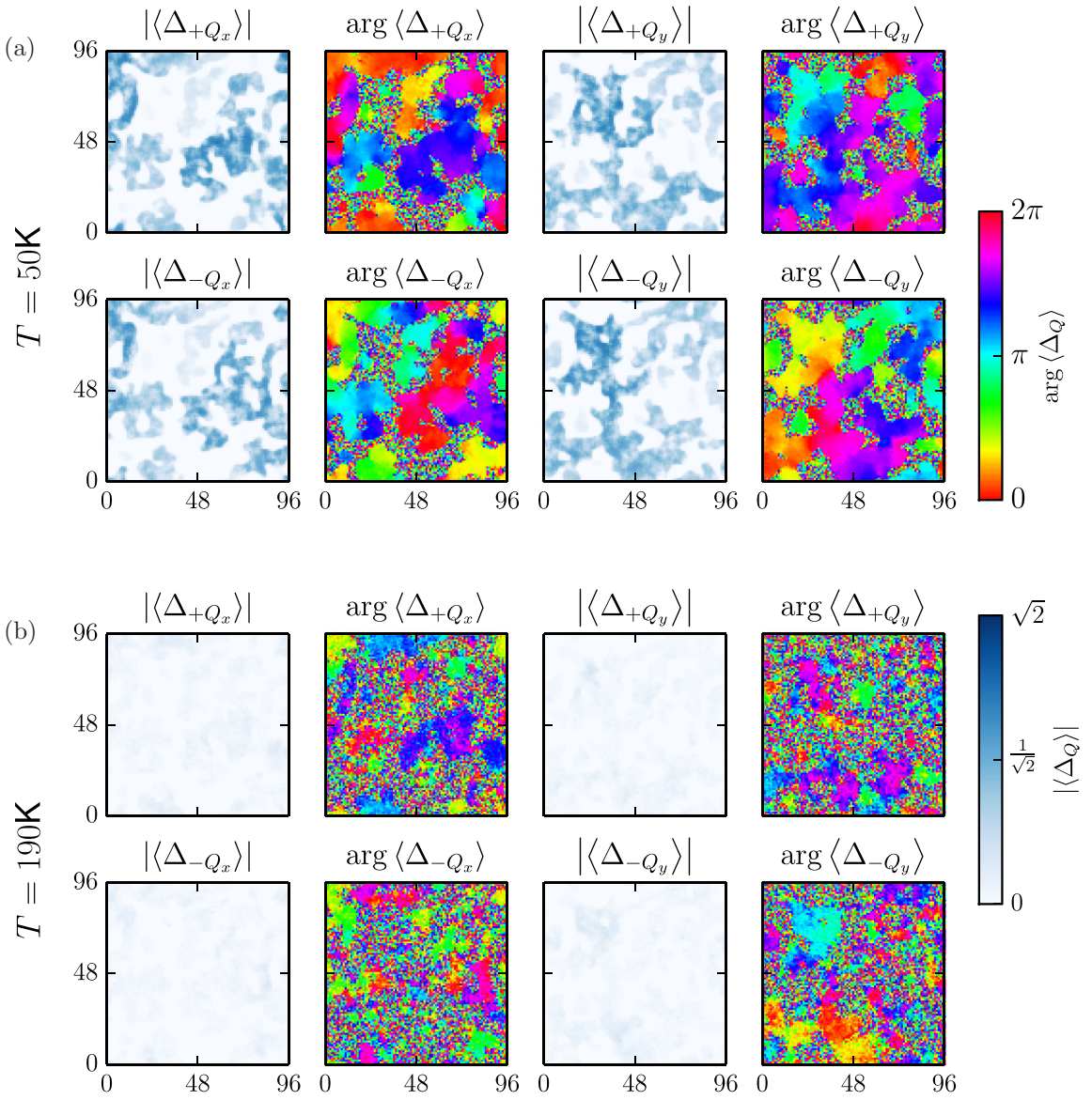

FIG. 8. Spatial variations of PDW components in the PSPN state at two temperatures: (a) $T = 50\,\mathrm{K} < T_{CO}$ and (b) $T = 190\,\mathrm{K} > T_{CO}$. In the same MC simulations in Fig. 6 using GL functional $F_{4,\mathrm{lattice}}$ [Eq. (10)], we measured the PDW order parameters $\langle\Delta_{\pm Q_{x,y}}\rangle$. At $T = 50\,\mathrm{K}$, some domains of directional PDW are wiped out owing to strong fluctuations in SC phases. At $T = 190\,\mathrm{K}$, the fluctuations are stronger and most of the PDW orders are destroyed. These results suggest the absence of PDW superconductivity irrespective of T_{CO}.

the section overview, these results point to a phase-separated directional PDW state. We found that using our model of PDW4 and RFD together with suitable parameters, we can reproduce the phase separation pattern for the directional CDW (see Fig. 3 in SM [98] for more details). We note that the REXS result [13] also supports such a phase separation picture for the directional CDW.

IV. CONSTRAINT FROM CDW WITH PREDOMINANTLY D-WAVE FORM FACTOR

Before the discussion of the spectral functions of the PDW system, we shall first figure out the pairing symmetry of the PDW. Both STM [20,56] and REXS [15] experiments strongly indicate that the CDW order within the pseudogap has a predominantly d-wave form factor. If we insist that the CDW order is only originated from the corresponding PDW order, then we need to understand how this CDW form factor would constrain the pairing symmetry of the PDW.

Here we propose that the PDW has a $s' \pm id$-symmetry. First we write down the definition of a generic SC order parameter at sites r_i and r_j

$$\Delta(r_1, r_2) = \sum_Q \left(\sum_k \Delta_Q(k) e^{ik(r_1 - r_2)} \right) e^{iQ\frac{r_1+r_2}{2}} \equiv \sum_Q \Delta_Q(r) e^{iQ\cdot R}, \tag{13}$$

in which we allow multiple components with different modulation wave vectors Q, which determine the modulation

in the average coordinate $R = \frac{1}{2}(r_1 + r_2)$, and their (orbital) pairing symmetries involving relative coordinate $r = r_1 - r_2$ are described by the form factor $\Delta_Q(k)$. We can similarly define the order parameter for charge modulations [20] by a simple replacement $\Delta \to \rho$. We note that the definition above only describe the order parameters of the PDW components Δ_Q spatially uniform in the average coordinate (i.e., Δ_Q is independent of R). If we want to include (slow) spatial variation in Δ_Q, we can add a spatial varying factor by the substitution $\Delta_Q(r) \to \Delta_Q(R) f_Q(r)$ with the form factor encoded in $f_Q(r)$. In this section, we shall consider spatially uniform case only.

The pairing symmetry factor for $+Q_x$ is assumed to be

$$\Delta_{+Q_x}(k) = \Delta_s\left(k_x^2 + k_y^2\right) + \Delta_d e^{i\phi}\left(k_x^2 - k_y^2\right), \tag{14}$$

where $\Delta_{s,d} \in \mathbb{R}$, $\phi \in [0, 2\pi)$. It is clear that the first (second) term is s wave (d wave). Here $\Delta_{s,d}$ and ϕ will be constrained by the CDW dominating d-wave form factor shown in the experiments. Time reversal symmetry requires that $\Delta_{-Q}(k) = \Delta^*_{+Q}(-k)$. By the relation $\rho_{2Q_a}(r) = \Delta^*_{-Q_a}(r)\Delta_{+Q_a}(r)$, the CDW form factor can be shown as (see Appendix)

$$\begin{aligned}\rho_{2Q_x}(k) = {} & \left(\Delta_s^2 + e^{2i\phi}\Delta_d^2/2\right)\underbrace{\left(k_x^2 + k_y^2\right)^2}_{s\text{-wave}} \\ & + \left(2e^{i\phi}\Delta_s\Delta_d\right)\underbrace{\left(k_x^2 + k_y^2\right)\left(k_x^2 - k_y^2\right)}_{d\text{-wave}} \\ & + \left(e^{2i\phi}\Delta_d^2/2\right)\underbrace{\left(k_x^4 - 6k_x^2k_y^2 + k_y^4\right)}_{g\text{-wave}}\end{aligned} \tag{15}$$

up to an overall factor. The STM experiment [20,56] reveals that the s-wave component is much smaller than the d-wave one, while the REXS experiment [15] shows that a pure d-wave CDW cannot fully reproduce the experimental data. Inspired by these experimental facts, we simply choose the s-wave component $\Delta_s^2 + \frac{1}{2}e^{2i\phi}\Delta_d^2$ to vanish, leaving only the d-wave and g-wave components. This particular choice requires $e^{i\phi} = \pm i$ and $\Delta_d/\Delta_s = \sqrt{2}$. Explicitly we take

$$\Delta_{sQ_a}(k) = \Delta_0\left[\left(k_x^2 + k_y^2\right) + is\sqrt{2}\left(k_x^2 - k_y^2\right)\right], \tag{16}$$

where $\Delta_0 \in \mathbb{C}$. Here Δ_{+Q_a} and Δ_{-Q_a} transform to each other under time reversal symmetry and we simply choose $\Delta_{sQ_x} \leftrightarrow \Delta_{sQ_y}$ related by a $\pi/2$ rotation. In the experiments, the d-wave form factor also indicates that the charge orders are located at the oxygen site. Therefore, in the (single band) model on a square lattice, we shall consider the (nearest neighbor) bond order between the lattice sites (with Cu atoms) to mimic this experimental fact, and we restrict ourselves to the $s' \pm id$-wave pairing symmetry

$$\frac{\Delta_{sQ_a}(k)}{\Delta_0} = (\cos k_x + \cos k_y) + is\sqrt{2}(\cos k_x - \cos k_y). \tag{17}$$

A detailed derivation of the induced CDW form factor for Eq. (17) is given in Appendix, in which we show that the above consideration remains valid in the lattice scenario.

V. QUASIPARTICLE SPECTRAL FUNCTIONS AND ARPES

In this section, we study the spectral functions of PDW systems and compare the results with the ARPES experiments. Many exotic properties are observed in ARPES. Early studies have revealed that the Fermi surface in the pseudogap forms the so-called Fermi arcs [12,51], disconnected segments of gapless quasiparticle excitations near the nodes. Near the antinodes, the spectrum is gapped, while the quasiparticle peak is very broad or even ill-defined [2]. Recently, it is found [54,55] that by comparing the data above and below T^*, the quasiparticle spectra have the feature of k_F-k_G misalignment near the antinodes, where k_F is the Fermi momentum for $T > T^*$ and k_G is the back-bending momentum for $T < T^*$. This feature cannot be explained by conventional SC pairing, otherwise we would expect $k_F = k_G$. Moreover, away from the antinode, the spectral gap is closed from below [55,101,102]. While from a calculation [47] for a model with pure CDW, an order observed in STM and REXS, shows that the spectral gap is closed from above and it fails to capture this ARPES feature. On the other hand, PDW models [47,48] can successfully capture the k_F-k_G misalignment and the feature of the gap closing from below, suggesting that PDW plays an important part in the pseudogap phenomenology.

To compute the spectral functions, we introduce a lattice Hamiltonian with PDW pairings [Eq. (18)] taking into account the spatial variations in the PDW order parameters, pairing symmetry and thermal (phase) fluctuations. In order to study separately the effects of the RFD induced random phases, phase separation, and the thermal fluctuations, we will consider four PDW systems: (i) uniform PDW2 with $s' \pm id$-wave pairing symmetry, (ii) $s' \pm id$-wave PDW2 with random phases induced by RFD, (iii) $s' \pm id$-wave PDW4 with phase separation in pairing amplitudes $\Delta_{x,y}$ but no random phase, and lastly (iv) PSPN state with thermal fluctuations in the PDW phases θ_{sQ_a}, originated from a $s' \pm id$-wave PDW4 state. For the former three systems, it is sufficient to compute the spectral functions by feeding a static PDW configuration into the Hamiltonian [Eq. (21)]. But for the last one, it is needed to incorporate disorder average and thermal fluctuations through a sequence of MC generated PDW configurations [Eq. (22)].

Actually there are similar studies on the effect of thermal fluctuations on the spectral features. In Ref. [103], the authors studied the thermal averaged spectral functions for cuprates within a spin liquid scenario, where the order parameter fluctuates between a d-wave superconductor and a nearby staggered-flux state related by SU(2) rotations. While in Ref. [104], the authors studied the fluctuating d-wave superconductor scenario, in which the SC phases are strongly disordered due to vortex proliferation. These studies also appear to reproduce the Fermi arc feature observed in ARPES.

We first write down the real space Hamiltonian $H = H_0 + H_\Delta$ with

$$\begin{aligned}H_0 &= -\sum_{\mathbf{i}\delta\sigma} t_\delta c^\dagger_{\mathbf{i}+\delta\sigma} c_{\mathbf{i}\sigma} + \text{H.c.} - \mu\sum_{\mathbf{i}\sigma} c^\dagger_{\mathbf{i}\sigma} c_{\mathbf{i}\sigma} \\ H_\Delta &= \sum_{ia} \Delta^*(\mathbf{i}+a,\mathbf{i})(c_{\mathbf{i}+a\uparrow}c_{\mathbf{i}\downarrow} - c_{\mathbf{i}+a\downarrow}c_{\mathbf{i}\uparrow}) + \text{H.c.},\end{aligned} \tag{18}$$

where $\Delta(\mathbf{i}+a,\mathbf{i})$ is the nearest neighbor singlet (bond) pairing with $a=\hat{x},\hat{y}$. The parameters are taken from Ref. [12] that (with lattice constant $a_0=1$) the nearest neighbor hopping $t_1=0.4$ eV, the next nearest neighbor hopping $t_2/t_1=-0.2$, and the third nearest neighbor hopping $t_3/t_1=0.05$. The PDW order parameters in momentum space $\Delta_{\pm Q_a}(k)$ describe pairing with total momentum $\pm Q_a$ and the pairing centers are at $\pm Q_a/2$. In order to explain the ARPES results, we follow Ref. [47] and choose the pairing centers at the Brillouin zone (BZ) boundary that $\pm Q_x/2=\pm(\pi,Q_0/2)$ and $\pm Q_y/2=\mp(Q_0/2,\pi)$ related by a $\pi/2$ rotation (see Fig. 1). In this study, we take the chemical potential $\mu/t_1\approx -0.758$ (corresponding hole doping $\approx$0.117) such that the electronic band intersects with the BZ boundary exactly at the aforementioned pairing centers with $Q_0=\pi/4$. The resultant PDW has a period of $8a_0$ and corresponding CDW with period $4a_0$. As (hole) doping increases, the corresponding CDW modulation $2Q_0$ decreases by choice [47], and this trend is in accord with the results observed in x-ray experiments [10,12,14].

In order to incorporate spatial nonuniform pairing order parameters, we generalize Eq. (13) to

$$\Delta(r_1,r_2)=\bar{\Delta}\sum_Q \Delta_Q(R)f_Q(r)e^{iQ\cdot R}, \tag{19}$$

where $R=\frac{1}{2}(r_1+r_2)$ is the average coordinate, $r=r_1-r_2$ is the relative coordinate, and $f_Q(r)$ describes the pairing symmetry in real space, given by [Eq. (17)]

$$f_{sQ_a}(r)=\begin{cases}1+is\sqrt{2}, & r=\pm\hat{x}\\ 1-is\sqrt{2}, & r=\pm\hat{y}\end{cases}. \tag{20}$$

Here the spatial dependent pairing order parameters $\Delta_Q(R)\in\mathbb{C}$ will be taken from the results of the MC simulations with spatial mean magnitude $\langle|\Delta_Q(R)|\rangle_R=1$. We shall assume that the orders are sufficiently smooth, and we can take the interpolation value $\Delta_Q(R)=\frac{1}{2}(\Delta_Q(r_1)+\Delta_Q(r_2))$ as the bond order parameters [105]. Finally, an overall scaling $\bar{\Delta}$ is added to control the "gap" size. In the following, we compute the quasiparticle spectral functions in momentum space corresponding to the Hamiltonian Eq. (18) according to

$$A_{\{\Delta\}}(k,\omega)=-\frac{1}{\pi}\mathrm{Im}\langle k|\frac{1}{\omega+i0^+-H_{\{\Delta\}}}|k\rangle, \tag{21}$$

provided that the pairing order parameters $\{\Delta\}=\{\Delta_{sQ_a}\}$ are given. Here $|k\rangle=\frac{1}{\sqrt{N}}\sum_{\mathbf{i}}e^{ik\cdot x_{\mathbf{i}}}|x_{\mathbf{i}}\rangle$ is the single-particle wave vector with momentum k in the first BZ.

A. PDW2

We start with the uniform $s'\pm id$-wave PDW2 system [Eq. (8), $\gamma_3^\Delta<0$]. In particular, we choose to add the $\Delta_{\pm Q_y}$ PDW orders, and the results of selected momentum line scans (see Fig. 1) are shown in Fig. 9(a). More line scans are shown in Fig. 5 of the SM [98]. We first notice that the Fermi surface is gapped at both the antinodal regions ($k_{x,y}=\pi$ scans), despite that we have only added the PDW pairings centered at $\pm Q_y/2$. The spectra near the nodal regions ($k_{x,y}=\frac{\pi}{2}$ scans) are gapless and resemble the bare spectra without the PDW pairing, except the existence of some gap structures away from the Fermi energy. These results constitute the Fermi arcs observed in the ARPES experiments [12,51]. Within the PDW picture, these Fermi surface segments are due to poor pairing condition near the Fermi surface. However, the "gap," defined as the energy gap at the back-bending momentum k_G below the chemical potential, is not monotonically decreasing from the antinodes [compare Fig. 5(a-IV) and (a-V) in the SM [98]]. This is however inconsistent with the ARPES [52,53]. Next, the band structures near two antinodes are different. Near $\pm Q_x/2$ [Fig. 9(a-III)], the spectrum resembles closely a conventional band structure gapped by an order parameter such that the lower band edge at ~ -0.2 eV is left below the Fermi energy. Near $\pm Q_y/2$ [Fig. 9(a-I)], where the PDW order is centered, we notice the so-called k_F-k_G misalignment of the band gap, where k_F is the Fermi momentum of gapless bare bands (white dashed lines) at high enough temperature. This misalignment observed in the ARPES experiments imposes a strong constraint on theories. Although this uniform PDW2 state can explain several important features observed in ARPES, more satisfactory results could be obtained for the systems we will consider below.

Next we turn to the $s'\pm id$-wave PDW2 system with RFD induced random phases. We set the amplitude $|\Delta_{\pm Q_y}(R)|$ to be constant and use the averaged phases in Fig. 3 obtained by MC simulation as input to compute the spectral functions. The results with the same line scans are shown in Fig. 9(b). The spectra are similar to those in the uniform PDW2 state, except a noticeable difference that the coherent peaks are more broadened near the pairing centers $\pm Q_y/2$ than at the other antinodal region $\pm Q_x/2$ [compare Fig. 9(b-I) and 9(b-III)]. Near the nodal regions, the spectra are largely unaltered by the random phases, except some minor spreading of the spectral weights. So the main effect of random phases is broadening of the coherent peaks near the pairing centers, and the band structure induced by the PDW orders is largely preserved.

B. Phase-separated PDW4

We now discuss the $s'\pm id$-wave PDW4 state with the $\Delta_{x,y}$-phase separation [Eq. (10), $\gamma_{2,3}^\Delta>0$]. Firstly, we notice that the PDW2 spectra in Fig. 9, especially near the antinodes, do not preserve the fourfold rotational symmetry, while this symmetry appears to be unspoiled in the ARPES results. In the following, we show that the RFD induced phase separation pattern for PDW4 can help to resolve this discrepancy, namely approximately preserving the fourfold rotational symmetry while still maintaining all the spectral features obtained in PDW2.

Here the PDW orders exists at all four momenta $\pm Q_{x,y}$. We take the averaged $\Delta_{x,y}$ amplitudes with phase separation in Fig. 5 as input to calculate the spectral functions. Also focusing on the effect of phase separation, we set the PDW phases as spatial independent (i.e., constant). The results of line scans $k_{x,y}=\pi$ are shown in Fig. 10(a), and more scans are presented in Fig. 6 of the SM [98]. PDW orders now exist at all four pairing centers $\pm Q_{x,y}/2$; the phase separated orders result in spectrum broadening near both antinodal regions. The effect of amplitude fluctuations in PDW4 is similar to that of phase fluctuations in PDW2 above in terms of spectrum broadening, except it affects both antinodal regions. The nodal Fermi surface is again gapless with minor peak broadening

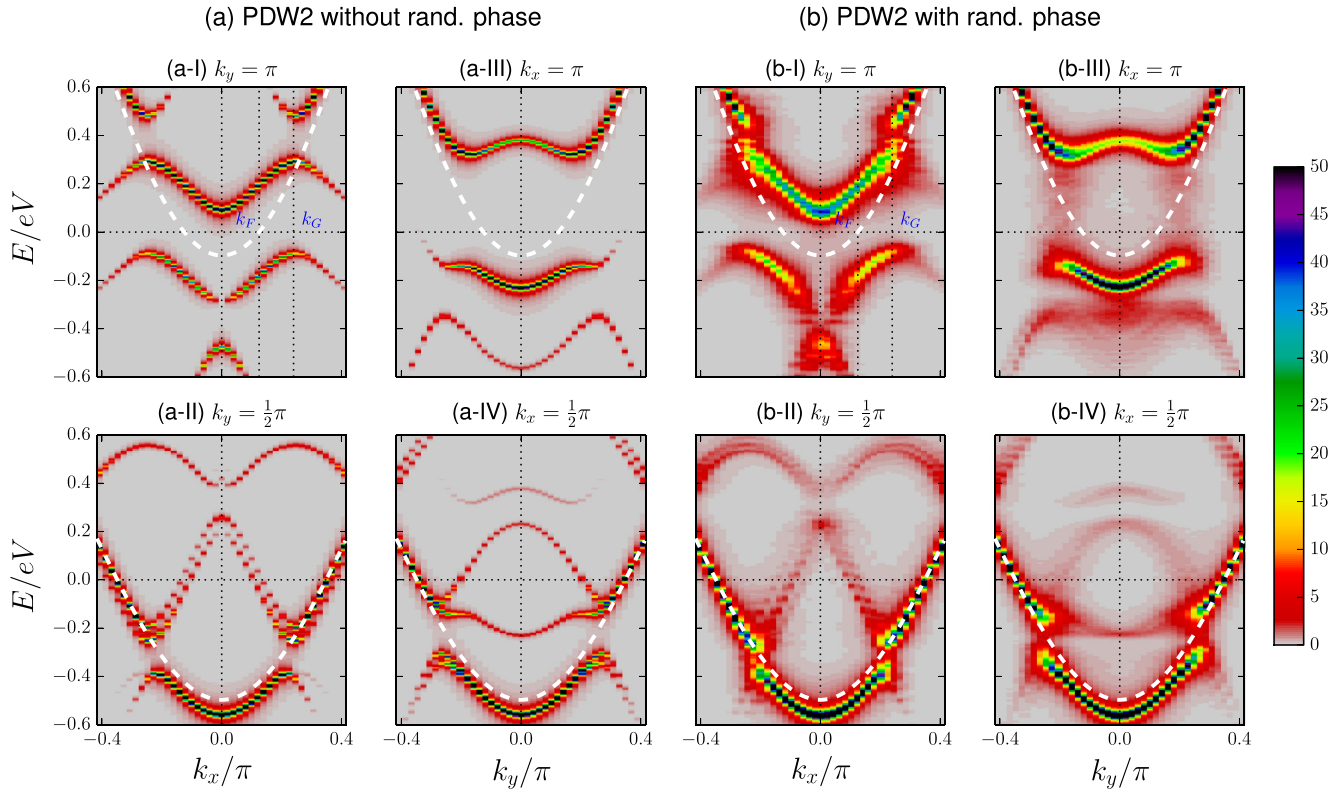

FIG. 9. Spectral functions at two line scans (see Fig. 1) in BZ. Panel (a) shows the PDW2 system without adding random phases and panel (b) shows the PDW2 with static random phases taken from Fig. 3. The PDW orders $\Delta_{\pm Q_y}$ are added at two pairing centers $\pm Q_y/2$. The white dashed lines represent the bare bands. Both systems show the k_F-k_G misalignment in the $k_y = \pi$ plots as seen in subplots (a-I) and (b-I), where k_F is the Fermi momentum of the bare band and k_G is the back bending momentum. But the spectra in the system with random phases are more broadened. We take $Q_0 = \pi/4$, $\tilde{\Delta} = 0.125$ eV, $t_1 = 0.4$ eV, $t_2/t_1 = -0.2$, $t_3/t_1 = 0.05$, and $\mu/t_1 \approx -0.758$. System size: 96×96 with periodic boundary condition. More line scans are provided in the Supplemental Material [98].

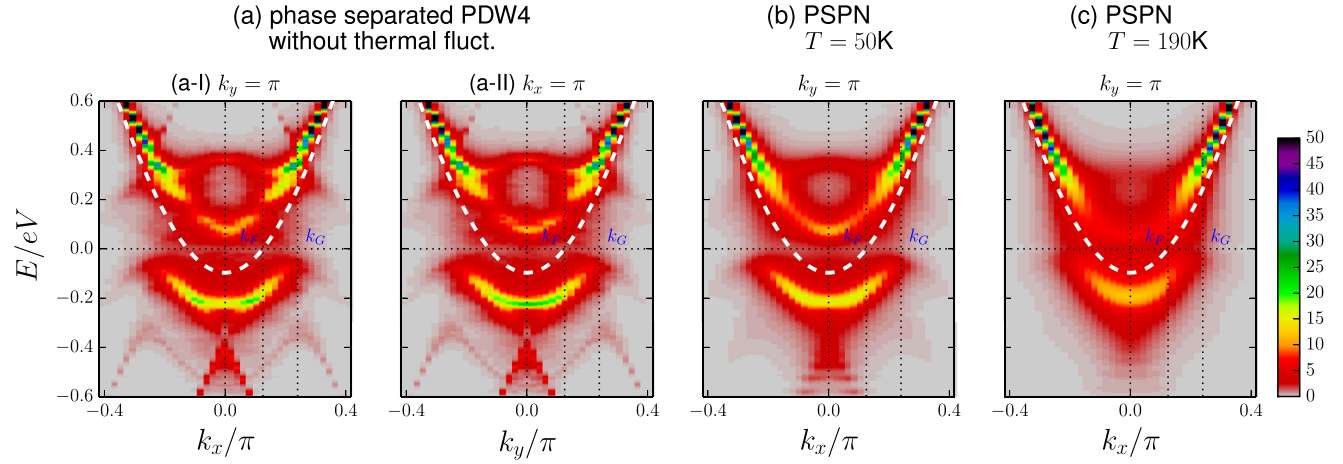

FIG. 10. Spectral functions for (a) phase-separated PDW4 without thermal fluctuations, (b) PSPN state with thermal fluctuations at $T = 50\,\mathrm{K} < T_{CO}$, and (c) PSPN state at $T = 190\,\mathrm{K} > T_{CO}$ are plotted at $k_{x,y} = \pi$. The PDW orders $\Delta_{\pm Q_{x,y}}$ are added at four pairing centers $\pm Q_{x,y}/2$. In panel (a), we take the averaged PDW amplitude results $|\Delta_{\pm Q_{x,y}}|$ from Fig. 5 as input and the PDW phases are homogeneous and constant. The spectra closely resemble superposition of two PDW2 spectra with either $\Delta_{\pm Q_x}$ or $\Delta_{\pm Q_y}$ and the fourfold rotational symmetry is approximately preserved. In panels (b) and (c), we have performed the thermal and disorder averages at the stated temperatures. We note that the spectrum superposition feature revealed in (a) remains. In all cases, the k_F-k_G misalignment feature is intact, though the broadening is more severe in the two high temperature cases. The parameters are the same as in Fig. 9. More line scans are provided in the Supplemental Material [98].

[Figs. 6(a-VII) and 6(a-XIV) in the SM [98]]. Next we observe that the spectra appear as a superposition of those from a PDW2 with $\Delta_{\pm Q_x}$ orders and another one with $\Delta_{\pm Q_y}$ orders (see Fig. 7 in the SM [98] for a detailed discussion) and thus approximately preserve the fourfold rotational symmetry. This is an intriguing result since the RFD induces directional PDW domains breaking the local fourfold rotational symmetry. We note that the spectra at $k_{x,y} = \pi$ [Fig. 10(a)] actually agree with the ARPES results [54,55] better than the PDW2's [Fig. 9(a-I)], in which the lower band edge near ~ -0.2 eV is missing. We also note that the dispersion approaches the Fermi level from below when moving from antinodes towards the nodal regions [see Figs. 6(a) and 8 in the SM [98]], consistent with ARPES results [55,101,102]. Near the end of the gapless Fermi arc (see Fig. 8 in the SM [98]), the dispersion is not particle-hole symmetric but bends downward and loses spectral weight, qualitatively consistent with the ARPES results by Yang *et al.* [101,102]. The same data, as well as some antinodal features, has also been nicely captured by the phenomenological YRZ model [102,106–108]. We have also performed a similar calculation on the PDW4 with coexisting $\Delta_{x,y}$ ($\gamma_2^{\Delta} < 0$); the spectrum does not have the superposition feature and fails to reproduce the ARPES results due to the strong interference effect of the Q_x and Q_y PDW orders.

C. PSPN state with (thermal) phase fluctuations

We are finally ready to discuss the spectral function results for the PSPN state with phase fluctuations. This state stems from the $s' \pm id$-wave PDW4 state. In order to capture the phase fluctuations of the PDW orders, it is insufficient to compute only the static averaged configurations as in above. Actually we need to compute the averaged qausiparticle spectral function over thermal fluctuations, given by [104]

$$\langle A(k,\omega)\rangle = \frac{\sum_{\{\Delta\}} A_{\{\Delta\}}(k,\omega) e^{-\frac{1}{k_B T} F_{4,\text{lattice}}}}{\sum_{\{\Delta\}} e^{-\frac{1}{k_B T} F_{4,\text{lattice}}}} \tag{22}$$

where for brevity $\{\Delta\}$ denotes $\{\Delta_{s Q_a}\}$. This averaged spectral function $\langle A(k,\omega)\rangle$ is calculated by taking the thermal average with $\{\Delta_{s Q_a}\}$ configurations generated by MC simulations of the GL functional $F_{4,\text{lattice}}$ in Eq. (10). We then perform the disorder average over 16 RFD configurations. We carry out the numerical calculations at two temperatures $T = 50$ K and $T = 190$ K, which are at opposite sides of the charge order crossover temperature of $T_{CO} \sim 150$ K. Again, for each RFD configuration, we take the amplitudes from the MC results with both amplitude and phase updates and simulated annealing process as in Fig. 5 as input and then carry out the MC simulations on the PDW phases at the desired temperatures. The results for 50 K and 190 K are, respectively, presented in Figs. 10(b) and 10(c). The spectra are smoothened compared to those without phase fluctuations, but the band structures are largely unaltered compared with the PDW4 results without phase fluctuations [Fig. 10(a)]. Many important features that we obtained previously remain intact even with the presence of the phase fluctuations. Firstly, the "Fermi arcs" remain. The spectra near the antinodes are severely broadened. Compared with the PDW4 results without phase fluctuations [Fig. 10(a)], the broadening mainly comes from the $\Delta_{x,y}$-phase separation instead of the phase fluctuations. The "gap" decreases monotonically away from the antinodes owing to the phase fluctuation induced gap fillings and finally becomes gapless near the nodal regions. Again away from antinodes, the spectrum approaches the Fermi level from below, in accord with ARPES experiments [55,101,102]. Secondly, the band structure superposition and the k_F-k_G misalignment also survive the phase fluctuations. Moreover, if we compare the results for 50 K and 190 K, we see that the crossover temperature T_{CO} does not induce a qualitative change on the spectrum. The two major features mentioned above still survive the depinning of the smectic phases across T_{CO} and can be regarded as definitive characteristics of the PDW orders for $T < T^*$. These results agree well with the ARPES measurements [12,52–55,109,110], in which these features are also shown in the pseudogap region below T^*. (We note that these ARPES features can also be captured to some extent by alternative theories [78,111].) Comparison of the result and the ARPES data is given in Fig. 9 of the SM [98].

By comparing the spectral results for different PDW states, we notice two major effects of RFD. Firstly, in terms of the phase separation pattern and the random phases, it broadens the spectrum, as one would have expected from a disordered system. The broadening is more severe near the antinodes, which is also observed in ARPES data [2]. But more importantly, RFD induces the phase separation pattern for the directional orders, rendering the spectra approximately obeying the fourfold symmetry, while still preserving many experimentally observed features appeared in the directional PDW2 state.

Lastly we argue that the superposition feature actually support the proposal that the cuprate SC has stripe PDW and CDW orders ($\gamma_2^{\Delta} > 0$). Since without PDW order, the fermionic spectrum in the CDW phase cannot reproduce the ARPES results [47,55,101,102] that the spectrum approaches from the Fermi level from below, we shall confine ourselves to various scenarios of PDW theories. First, the pure PDW2 could not reproduce the lower band edge of the ARPES spectrum as we discussed above. Next, we have also checked that the checkerboard PDW4 state with $\gamma_{2,3}^{\Delta} < 0$ could not reproduce the ARPES results. A third possibility is proposed in Ref. [47] that the ARPES results actually constitute from a checkerboard PDW4 orders decaying in the momentum space. It is proposed that the PDW symmetry factor $f_{s Q_a}(k) \sim e^{-k^2/\xi^2}$ decays away from the pairing centers, and it can successfully explain the k_F-k_G misalignment and the Fermi arcs. But the spectrum is largely coming from the PDW2 states at the pairing centers due to the exponential decaying SC symmetry factor, so it has missed the ARPES feature at the lower band edge shown in Fig. 10(a-I). Nevertheless, the stripe PDW does not necessarily need to exist within the same layer. Actually, alternating layers of x- and y-directional stripe PDW [40] would produce a similar superposition spectra. But the phase separation structure similar to those in Fig. 5 is indeed observed in STM [19,56] and also supported by REXS [13], so it is perhaps favored over the alternating layer scenario. It is hard to exhaust all the possibilities, but it is intriguing to see the convergence of the STM, REXS (indicating stripe CDW, induced by the stripe PDW), and the ARPES (indicating stripe PDW) experimental results towards a unifying theoretical framework.

VI. CONCLUSIONS

In conclusion, the phase separated pair nematic (PSPN) state derived from a four-component pair density wave (PDW) model under the influence of random field disorders (RFD) captures coherently a number of experimental results in the pseudogap. We consider a parameter regime $\gamma_{2,3}^{\Delta} > 0$ for the phenomenology of cuprates, in which all the PDW components $\Delta_{\pm Q_a}$ are competing with each other. The new choice of parameter impedes the generalization of existing PDW results to the present case, however, we show that in terms of a phenomenological GL approach, the experimental observed features obtained in the existing PDW theory are retained if disorders are included. It is shown that CDW and a time-reversal symmetry breaking (TRSB) order in the form of loop current (LC) are induced as secondary composite orders. The inclusion of disorders permits the state to be spatially inhomogeneous (in terms of the PDW components), and this readily resolves an issue concerning the incompatibility of CDW and loop current order within a four-component PDW model [48]. Nonetheless, the CDW is short ranged under the influence of random field disorders, consistent with the STM [19,20,56] and REXS [13] results, while the LC order can account for the TRSB order observed in polar Kerr rotation [25,26] and polarized neutron diffraction [27–30] experiments. Furthermore, by a MC simulation, we show that random field disorders can also induce a phase separation pattern for the CDW, similar to that observed in STM. This PSPN state also appears to capture other experimental features. It explains a distinct temperature scale $T_{CO} < T^*$ for the static (short range) CDW (see Sec. III). More importantly, it accounts for the same pseudogap temperature T^* observed in linear resistivity, ARPES (for the anomalous spectral features), REXS (for the dynamically fluctuating directional CDW), and polarized neutron diffraction (for the IUC TRSB order) experiments. We also argue that the thermal superconducting phase fluctuations lead to finite flux flow resistance, resulting in a nonsuperconducting state regardless of T_{CO}. To test the proposed PDW theory, one may probe the half SC flux trapped at the 2π-CDW dislocation (see Secs. II A and III A), provided that the local SC phase is strongly pinned. In Sec. IV, we constrain the PDW, from the observed CDW with a predominantly d-wave form factor, to have $s' \pm id$ pairing symmetries. In Sec. V, we show that a number of anomalous features in ARPES, namely Fermi arcs, k_F-k_G misalignment, and antinodal gap closing from below are retained in the PSPN state, even with thermal fluctuations. Moreover, the PSPN state is shown to have severe coherent peak broadening near the antinodes (but not the nodes), which has been a puzzling feature observed in ARPES [2]. The random field disorder induced phase separation pattern helps to explain why the ARPES spectrum still obey the fourfold rotational symmetry approximately, while locally it has been broken as revealed in STM. From above, we see that the random field disorders assist in understanding the pseudogap for $T < T^*$ in terms of the PSPN state by resolving several issues in previous studies.

ACKNOWLEDGMENTS

C.C. acknowledges useful discussions with Zheng-Xin Liu, Luyang Wang, and Zi-Xiang Li and helpful comments from Marc-Henri Julien. The author would also like to thank Hong Yao for previous collaboration on a related topic and Patrick A. Lee for his stimulating talk at the HKUST IAS 2014 program "topological matter, superconductivity and Majorana," which inspired the present work. Last but not least, the criticisms, suggestions and comments raised by the anonymous referees, especially the "First Referee," for improving the manuscript to the current form are highly appreciated.

APPENDIX: CDW FORM FACTOR INDUCED BY $s' \pm id$ PDW ON A SQUARE LATTICE

From the definitions of PDW Eq. (13) with symmetry factor Eq. (14)

$$f_{+Q}(k) = \left(k_x^2 + k_y^2\right) + \alpha\left(k_x^2 - k_y^2\right)$$
$$f_{-Q}(k) = f_{+Q}^*(k)$$

(here $\alpha \in \mathbb{C}$) and its induced CDW

$$\rho(r, +2Q) = \Delta^*(r, -Q)\Delta(r, +Q)\,,$$

we have

$$\rho(r,2Q) \propto \sum_{k_1 k_2} f_{+Q}(k_1) f_{+Q}(k_2) e^{-ik_1 r} e^{+ik_2 r}$$
$$= \sum_p \rho_{2Q}(p) e^{-ipr}\,,$$

and

$$\rho_{2Q}(p) = \int_0^{2\pi} d\theta_q\, f_{+Q}(q + p/2) f_{+Q}(q - p/2)$$

where $\theta_q = \arg q$, and we define $k_1 = q + \frac{p}{2}$ and $k_2 = q - \frac{p}{2}$. After some straightforward calculations, we have

$$\rho_{2Q}(p) = \frac{1}{8\pi}\Big[(1 + \alpha^2/2)\left(p_x^2 + p_y^2\right)^2$$
$$+ 2\alpha\left(p_x^2 + p_y^2\right)\left(p_x^2 - p_y^2\right)$$
$$+ (\alpha^2/2)\left(p_x^4 - 6p_x^2 p_y^2 + p_y^4\right)\Big] + \mathcal{O}(p^2).$$

We note that the first term is clearly s-wave, while the second (third) term is d-wave (g-wave) due to the identities $\cos 2\theta_p = \frac{p_x^2 - p_y^2}{p_x^2 + p_y^2}$ and $\cos 4\theta_p = \frac{p_x^4 - 6p_x^2 p_y^2 + p_y^4}{(p_x^2 + p_y^2)^2}$. A less rigorous derivation by the product of the basis functions

$$\rho_{2Q}(p) \sim (1 + \alpha \cos 2\theta_p)^2$$
$$= (1 + \alpha^2/2) + 2\alpha \cos 2\theta_p + (\alpha^2/2)\cos 4\theta_p$$

would also give the same result.

Similarly, in the lattice case, we have symmetry factor Eq. (17)

$$f(\vec{k}) = (\cos k_x + \cos k_y) + i\sqrt{2}(\cos k_x - \cos k_y).$$

Then

$$\rho(p,2Q) = \sum_q [(-1 + 2\sqrt{2}i)\cos k_{1x} \cos k_{2x}$$
$$+ (-1 - 2\sqrt{2}i)\cos k_{1y} \cos k_{2y}$$
$$+ 3\cos k_{1x} \cos k_{2y} + 3\cos k_{1y} \cos k_{2x}].$$

Then we substitute $k_1 = q + \frac{p}{2}$, $k_2 = q - \frac{p}{2}$ and evaluate the integrals $\sum_q \to \int_{-\pi}^{\pi} dq_x \int_{-\pi}^{\pi} dq_y$, and we have

$$\rho(p,2Q) = +\Delta_d^{\text{lat}}(\cos p_x - \cos p_y) + \Delta_g^{\text{lat}}(\cos p_x + \cos p_y),$$

where $\Delta_d^{\text{lat}} = 4\sqrt{2}\pi^2 i$ and $\Delta_g^{\text{lat}} = -2\pi^2$. In the continuous case, after setting the s'-wave component to zero, we have

$$\rho_{2Q}(k) = 2\sqrt{2}i\,\Delta_s^2\left(k_x^4 - k_y^2\right) - \Delta_s^2\left(k_x^4 - 6k_x^2k_y^2 + k_y^4\right).$$

The ratio of the d-wave to g-wave component is $-2\sqrt{2}i$, which matches that of the lattice case $\Delta_d^{\text{lat}}/\Delta_g^{\text{lat}} = -2\sqrt{2}i$. We note that although the *induced* CDW's form factor has a "g-wave" component, it manifests as s'-wave $\sim \cos p_x + \cos p_y$ due to the choice of nearest neighbor bond order and the square lattice.

[1] J. G. Bednorz and K. A. Müller, Zeitschrift für Phys. B Condens. Matter **64**, 189 (1986).
[2] J. Orenstein and A. J. Millis, Science **288**, 468 (2000).
[3] V. J. Emery and S. A. Kivelson, Nature (London) **374**, 434 (1995).
[4] M. Franz and A. J. Millis, Phys. Rev. B **58**, 14572 (1998).
[5] P. A. Lee, N. Nagaosa, and X.-G. Wen, Rev. Mod. Phys. **78**, 17 (2006).
[6] A. Perali, P. Pieri, G. C. Strinati, and C. Castellani, Phys. Rev. B **66**, 024510 (2002).
[7] G. Ghiringhelli, M. Le Tacon, M. Minola, S. Blanco-Canosa, C. Mazzoli, N. B. Brookes, G. M. De Luca, A. Frano, D. G. Hawthorn, F. He, T. Loew, M. M. Sala, D. C. Peets, M. Salluzzo, E. Schierle, R. Sutarto, G. A. Sawatzky, E. Weschke, B. Keimer, and L. Braicovich, Science **337**, 821 (2012).
[8] J. Chang, E. Blackburn, A. T. Holmes, N. B. Christensen, J. Larsen, J. Mesot, R. Liang, D. A. Bonn, W. N. Hardy, A. Watenphul, M. v. Zimmermann, E. M. Forgan, and S. M. Hayden, Nat. Phys. **8**, 871 (2012).
[9] A. J. Achkar, R. Sutarto, X. Mao, F. He, A. Frano, S. Blanco-Canosa, M. Le Tacon, G. Ghiringhelli, L. Braicovich, M. Minola, M. Moretti Sala, C. Mazzoli, R. Liang, D. A. Bonn, W. N. Hardy, B. Keimer, G. A. Sawatzky, and D. G. Hawthorn, Phys. Rev. Lett. **109**, 167001 (2012).
[10] E. Blackburn, J. Chang, M. Hücker, A. T. Holmes, N. B. Christensen, R. Liang, D. A. Bonn, W. N. Hardy, U. Rütt, O. Gutowski, M. v. Zimmermann, E. M. Forgan, and S. M. Hayden, Phys. Rev. Lett. **110**, 137004 (2013).
[11] S. Blanco-Canosa, A. Frano, T. Loew, Y. Lu, J. Porras, G. Ghiringhelli, M. Minola, C. Mazzoli, L. Braicovich, E. Schierle, E. Weschke, M. Le Tacon, and B. Keimer, Phys. Rev. Lett. **110**, 187001 (2013).
[12] R. Comin, A. Frano, M. M. Yee, Y. Yoshida, H. Eisaki, E. Schierle, E. Weschke, R. Sutarto, F. He, A. Soumyanarayanan, Y. He, M. Le Tacon, I. S. Elfimov, J. E. Hoffman, G. A. Sawatzky, B. Keimer, and A. Damascelli, Science **343**, 390 (2014).
[13] R. Comin, R. Sutarto, E. H. da Silva Neto, L. Chauviere, R. Liang, W. N. Hardy, D. A. Bonn, F. He, G. A. Sawatzky, and A. Damascelli, Science **347**, 1335 (2015).
[14] E. H. da Silva Neto, P. Aynajian, A. Frano, R. Comin, E. Schierle, E. Weschke, A. Gyenis, J. Wen, J. Schneeloch, Z. Xu, S. Ono, G. Gu, M. Le Tacon, and A. Yazdani, Science **343**, 393 (2014).
[15] R. Comin, R. Sutarto, F. He, E. H. da Silva Neto, L. Chauviere, A. Frano, R. Liang, W. N. Hardy, D. A. Bonn, Y. Yoshida, H. Eisaki, A. J. Achkar, D. G. Hawthorn, B. Keimer, G. A. Sawatzky, and A. Damascelli, Nat. Mater. **14**, 796 (2015).
[16] W. D. Wise, M. C. Boyer, K. Chatterjee, T. Kondo, T. Takeuchi, H. Ikuta, Y. Wang, and E. W. Hudson, Nat. Phys. **4**, 696 (2008).
[17] C. V. Parker, P. Aynajian, E. H. da Silva Neto, A. Pushp, S. Ono, J. Wen, Z. Xu, G. Gu, and A. Yazdani, Nature (London) **468**, 677 (2010).
[18] M. J. Lawler, K. Fujita, J. Lee, A. R. Schmidt, Y. Kohsaka, C. K. Kim, H. Eisaki, S. Uchida, J. C. Davis, J. P. Sethna, and E.-A. Kim, Nature (London) **466**, 347 (2010).
[19] A. Mesaros, K. Fujita, H. Eisaki, S. Uchida, J. C. Davis, S. Sachdev, J. Zaanen, M. J. Lawler, and E.-A. Kim, Science **333**, 426 (2011).
[20] K. Fujita, M. H. Hamidian, S. D. Edkins, C. K. Kim, Y. Kohsaka, M. Azuma, M. Takano, H. Takagi, H. Eisaki, S.-I. Uchida, A. Allais, M. J. Lawler, E.-A. Kim, S. Sachdev, and J. C. S. Davis, Proc. Natl. Acad. Sci. USA **111**, E3026 (2014).
[21] T. Wu, H. Mayaffre, S. Kramer, M. Horvatic, C. Berthier, W. N. Hardy, R. Liang, D. A. Bonn, and M.-H. Julien, Nature (London) **477**, 191 (2011).
[22] T. Wu, H. Mayaffre, S. Krämer, M. Horvatić, C. Berthier, W. N. Hardy, R. Liang, D. A. Bonn, and M.-H. Julien, Nat. Commun. **6**, 6438 (2015).
[23] S. A. Kivelson, E. Fradkin, and V. J. Emery, Nature (London) **393**, 550 (1998).
[24] A. Bianconi, A. Valletta, A. Perali, and N. L. Saini, Phys. C Supercond. **296**, 269 (1998).
[25] J. Xia, E. Schemm, G. Deutscher, S. A. Kivelson, D. A. Bonn, W. N. Hardy, R. Liang, W. Siemons, G. Koster, M. M. Fejer, and A. Kapitulnik, Phys. Rev. Lett. **100**, 127002 (2008).
[26] H. Karapetyan, J. Xia, M. Hücker, G. D. Gu, J. M. Tranquada, M. M. Fejer, and A. Kapitulnik, Phys. Rev. Lett. **112**, 047003 (2014).
[27] B. Fauqué, Y. Sidis, V. Hinkov, S. Pailhès, C. T. Lin, X. Chaud, and P. Bourges, Phys. Rev. Lett. **96**, 197001 (2006).
[28] Y. Li, V. Baledent, N. Barisic, Y. Cho, B. Fauque, Y. Sidis, G. Yu, X. Zhao, P. Bourges, and M. Greven, Nature (London) **455**, 372 (2008).
[29] L. Mangin-Thro, Y. Sidis, A. Wildes, and P. Bourges, Nat. Commun. **6**, 7705 (2015).
[30] V. Balédent, B. Fauqué, Y. Sidis, N. B. Christensen, S. Pailhès, K. Conder, E. Pomjakushina, J. Mesot, and P. Bourges, Phys. Rev. Lett. **105**, 027004 (2010).
[31] V. Hinkov, P. Bourges, S. Pailhes, Y. Sidis, A. Ivanov, C. D. Frost, T. G. Perring, C. T. Lin, D. P. Chen, and B. Keimer, Nat. Phys. **3**, 780 (2007).

[32] R. Daou, J. Chang, D. LeBoeuf, O. Cyr-Choiniere, F. Laliberte, N. Doiron-Leyraud, B. J. Ramshaw, R. Liang, D. A. Bonn, W. N. Hardy, and L. Taillefer, Nature (London) **463**, 519 (2010).

[33] Y. Lubashevsky, L. D. Pan, T. Kirzhner, G. Koren, and N. P. Armitage, Phys. Rev. Lett. **112**, 147001 (2014).

[34] O. Cyr-Choinière, G. Grissonnanche, S. Badoux, J. Day, D. A. Bonn, W. N. Hardy, R. Liang, N. Doiron-Leyraud, and L. Taillefer, Phys. Rev. B **92**, 224502 (2015).

[35] P. Fulde and R. A. Ferrell, Phys. Rev. **135**, A550 (1964).

[36] A. I. Larkin and Y. N. Ovchinnikov, Sov. Phys. JETP **20**, 762 (1965).

[37] A. Himeda, T. Kato, and M. Ogata, Phys. Rev. Lett. **88**, 117001 (2002).

[38] S. A. Kivelson, I. P. Bindloss, E. Fradkin, V. Oganesyan, J. M. Tranquada, A. Kapitulnik, and C. Howald, Rev. Mod. Phys. **75**, 1201 (2003).

[39] H.-D. Chen, O. Vafek, A. Yazdani, and S.-C. Zhang, Phys. Rev. Lett. **93**, 187002 (2004).

[40] E. Berg, E. Fradkin, E.-A. Kim, S. A. Kivelson, V. Oganesyan, J. M. Tranquada, and S. C. Zhang, Phys. Rev. Lett. **99**, 127003 (2007).

[41] D. F. Agterberg and H. Tsunetsugu, Nat. Phys. **4**, 639 (2008).

[42] K. Seo, H.-D. Chen, and J. Hu, Phys. Rev. B **78**, 094510 (2008).

[43] E. Berg, E. Fradkin, and S. A. Kivelson, Phys. Rev. B **79**, 064515 (2009).

[44] E. Berg, E. Fradkin, S. A. Kivelson, and J. M. Tranquada, New J. Phys. **11**, 115004 (2009).

[45] E. Berg, E. Fradkin, and S. A. Kivelson, Nat. Phys. **5**, 830 (2009).

[46] E. Fradkin, S. A. S. Kivelson, and J. M. J. Tranquada, Rev. Mod. Phys. **87**, 457 (2015).

[47] P. A. Lee, Phys. Rev. X **4**, 031017 (2014).

[48] D. F. Agterberg, D. S. Melchert, and M. K. Kashyap, Phys. Rev. B **91**, 054502 (2015).

[49] M. E. Simon and C. M. Varma, Phys. Rev. Lett. **89**, 247003 (2002).

[50] C. M. Varma, J. Phys. Condens. Matter **26**, 505701 (2014).

[51] M. R. Norman, H. Ding, M. Randeria, J. C. Campuzano, T. Yokoya, T. Takeuchi, T. Takahashi, T. Mochiku, K. Kadowaki, P. Guptasarma, and D. G. Hinks, Nature (London) **392**, 157 (1998).

[52] W. S. Lee, I. M. Vishik, K. Tanaka, D. H. Lu, T. Sasagawa, N. Nagaosa, T. P. Devereaux, Z. Hussain, and Z.-X. Shen, Nature (London) **450**, 81 (2007).

[53] T. Kondo, R. Khasanov, T. Takeuchi, J. Schmalian, and A. Kaminski, Nature (London) **457**, 296 (2009).

[54] M. Hashimoto, R.-H. He, K. Tanaka, J.-P. Testaud, W. Meevasana, R. G. Moore, D. Lu, H. Yao, Y. Yoshida, H. Eisaki, T. P. Devereaux, Z. Hussain, and Z.-X. Shen, Nat. Phys. **6**, 414 (2010).

[55] R.-H. He, M. Hashimoto, H. Karapetyan, J. D. Koralek, J. P. Hinton, J. P. Testaud, V. Nathan, Y. Yoshida, H. Yao, K. Tanaka, W. Meevasana, R. G. Moore, D. H. Lu, S.-K. Mo, M. Ishikado, H. Eisaki, Z. Hussain, T. P. Devereaux, S. A. Kivelson, J. Orenstein, A. Kapitulnik, and Z.-X. Shen, Science **331**, 1579 (2011).

[56] M. H. Hamidian, S. D. Edkins, C. K. Kim, J. C. Davis, A. P. Mackenzie, H. Eisaki, S. Uchida, M. J. Lawler, E.-A. Kim, S. Sachdev, and K. Fujita, Nat. Phys. **12**, 150 (2016).

[57] S. Gerber, H. Jang, H. Nojiri, S. Matsuzawa, H. Yasumura, D. A. Bonn, R. Liang, W. N. Hardy, Z. Islam, A. Mehta, S. Song, M. Sikorski, D. Stefanescu, Y. Feng, S. A. Kivelson, T. P. Devereaux, Z.-X. Shen, C.-C. Kao, W.-S. Lee, D. Zhu, and J.-S. Lee, Science **350**, 949 (2015).

[58] G. Grissonnanche, F. Laliberte, S. Dufour-Beausejour, A. Riopel, S. Badoux, M. Caouette-Mansour, M. Matusiak, A. Juneau-Fecteau, P. Bourgeois-Hope, O. Cyr-Choiniere, J. Baglo, B. Ramshaw, R. Liang, D. Bonn, W. Hardy, S. Kramer, D. LeBoeuf, D. Graf, N. Doiron-Leyraud, and L. Taillefer, arXiv:1508.05486.

[59] J. Chang, E. Blackburn, O. Ivashko, A. T. Holmes, N. B. Christensen, M. Hucker, R. Liang, D. A. Bonn, W. N. Hardy, U. Rutt, M. v. Zimmermann, E. M. Forgan, and S. M. Hayden, Nat. Commun. **7**, 11494 (2016).

[60] Y. Ando, S. Komiya, K. Segawa, S. Ono, and Y. Kurita, Phys. Rev. Lett. **93**, 267001 (2004).

[61] R. Daou, N. Doiron-Leyraud, D. LeBoeuf, S. Y. Li, F. Laliberte, O. Cyr-Choiniere, Y. J. Jo, L. Balicas, J.-Q. Yan, J.-S. Zhou, J. B. Goodenough, and L. Taillefer, Nat. Phys. **5**, 31 (2009).

[62] A. I. Larkin, Sov. Phys. JETP **31**, 784 (1970).

[63] Y. Imry and S.-k. Ma, Phys. Rev. Lett. **35**, 1399 (1975).

[64] L. Nie, G. Tarjus, and S. A. Kivelson, Proc. Natl. Acad. Sci. USA **111**, 7980 (2014).

[65] D. F. Mross and T. Senthil, Phys. Rev. X **5**, 031008 (2015).

[66] S. Sachdev, Sci. **288**, 475 (2000).

[67] T. Valla, A. V. Fedorov, P. D. Johnson, B. O. Wells, S. L. Hulbert, Q. Li, G. D. Gu, and N. Koshizuka, Science **285**, 2110 (1999).

[68] D. van der Marel, H. J. A. Molegraaf, J. Zaanen, Z. Nussinov, F. Carbone, A. Damascelli, H. Eisaki, M. Greven, P. H. Kes, and M. Li, Nature (London) **425**, 271 (2003).

[69] A. J. Achkar, F. He, R. Sutarto, C. McMahon, M. Zwiebler, M. Hucker, G. D. Gu, R. Liang, D. A. Bonn, W. N. Hardy, J. Geck, and D. G. Hawthorn, Nat. Mater. **15**, 616 (2016).

[70] K. B. Efetov, H. Meier, and C. Pepin, Nat. Phys. **9**, 442 (2013).

[71] L. E. Hayward, D. G. Hawthorn, R. G. Melko, and S. Sachdev, Science **343**, 1336 (2014).

[72] A. J. Achkar, X. Mao, C. McMahon, R. Sutarto, F. He, R. Liang, D. A. Bonn, W. N. Hardy, and D. G. Hawthorn, Phys. Rev. Lett. **113**, 107002 (2014).

[73] G. Campi, A. Bianconi, N. Poccia, G. Bianconi, L. Barba, G. Arrighetti, D. Innocenti, J. Karpinski, N. D. Zhigadlo, S. M. Kazakov, M. Burghammer, M. v. Zimmermann, M. Sprung, and A. Ricci, Nature (London) **525**, 359 (2015).

[74] P. Corboz, T. M. Rice, and M. Troyer, Phys. Rev. Lett. **113**, 046402 (2014).

[75] M. A. Metlitski and S. Sachdev, Phys. Rev. B **82**, 075128 (2010).

[76] C. Pépin, V. S. de Carvalho, T. Kloss, and X. Montiel, Phys. Rev. B **90**, 195207 (2014).

[77] Y. Wang, D. F. Agterberg, and A. Chubukov, Phys. Rev. B **91**, 115103 (2015).

[78] Y. Wang, D. F. Agterberg, and A. Chubukov, Phys. Rev. Lett. **114**, 197001 (2015).

[79] H. Freire, V. S. de Carvalho, and C. Pépin, Phys. Rev. B **92**, 045132 (2015).

[80] A. Perali, C. Castellani, C. Di Castro, and M. Grilli, Phys. Rev. B **54**, 16216 (1996).

[81] M. J. P. Gingras and D. A. Huse, Phys. Rev. B **53**, 15193 (1996).

[82] C. Zeng, P. L. Leath, and D. S. Fisher, Phys. Rev. Lett. **82**, 1935 (1999).
[83] G. Blatter, M. V. Feigel'man, V. B. Geshkenbein, A. I. Larkin, and V. M. Vinokur, Rev. Mod. Phys. **66**, 1125 (1994).
[84] G. Grüner, Rev. Mod. Phys. **60**, 1129 (1988).
[85] L. Radzihovsky and J. Toner, Phys. Rev. Lett. **78**, 4414 (1997).
[86] L. Radzihovsky and J. Toner, Phys. Rev. Lett. **79**, 4214 (1997).
[87] L. Radzihovsky and J. Toner, Phys. Rev. B **60**, 206 (1999).
[88] V. Berezinskii, Sov. Phys. JETP **32**, 493 (1971).
[89] D. J. Kosterlitz, J. M.; Thouless, J. Phys. C Solid State Phys. **6**, 1181 (1973).
[90] L. Radzihovsky and A. Vishwanath, Phys. Rev. Lett. **103**, 010404 (2009).
[91] L. Radzihovsky, Phys. Rev. A **84**, 023611 (2011).
[92] D. G. Barci and E. Fradkin, Phys. Rev. B **83**, 100509 (2011).
[93] J. A. Robertson, S. A. Kivelson, E. Fradkin, A. C. Fang, and A. Kapitulnik, Phys. Rev. B **74**, 134507 (2006).
[94] A. Del Maestro, B. Rosenow, and S. Sachdev, Phys. Rev. B **74**, 024520 (2006).
[95] Y. Wang, A. Chubukov, and R. Nandkishore, Phys. Rev. B **90**, 205130 (2014).
[96] M. Gradhand, I. Eremin, and J. Knolle, Phys. Rev. B **91**, 060512 (2015).
[97] More precisely, γ_4^{Δ} controls the phase coherence between the induced directional charge-4e SC $\Delta_{4e}^{a} = \Delta_{+Q_a}\Delta_{-Q_a}$. Choosing $\gamma_4^{\Delta} = 0$ destroys the phase coherence and results in a phase separation in the directional charge-4e SC. More detailed discussion is given in Sec. I of the Supplemental Material [98].
[98] See Supplemental Material at http://link.aps.org/supplemental/10.1103/PhysRevB.93.184514 for numerically computed correlations in directional CDW and charge-4e SC, comparisons with experimental data, and more details on the superposition feature of the spectral functions.
[99] This threshold is set in analog of the MC study of the BKT transition, in which a *global* order parameter $\bar{\Delta} = \langle |N^{-1}\sum_{\mathbf{i}} e^{i\theta(\mathbf{i})}| \rangle$ is used (θ is the XY phase and N is number of sites). Near the BKT transition temperature, there is a sharp drop in $\bar{\Delta}$ from 0.6 to 0.2. Thus for $\bar{\Delta} \gtrsim 0.2$, the system is regarded as in the short-range correlated phase.
[100] Y. B. Kim, C. F. Hempstead, and A. R. Strnad, Phys. Rev. **139**, A1163 (1965).
[101] H.-B. Yang, J. D. Rameau, P. D. Johnson, T. Valla, A. Tsvelik, and G. D. Gu, Nature (London) **456**, 77 (2008).
[102] H.-B. Yang, J. D. Rameau, Z.-H. Pan, G. D. Gu, P. D. Johnson, H. Claus, D. G. Hinks, and T. E. Kidd, Phys. Rev. Lett. **107**, 047003 (2011).
[103] S. Bieri and D. A. Ivanov, Phys. Rev. B **79**, 174518 (2009).
[104] Q. Han, T. Li, and Z. D. Wang, Phys. Rev. B **82**, 052503 (2010).
[105] We note that the order parameters of the PDW components $\Delta_Q(R)$ in the Hamiltonian Eq. (18) actually take values at the bond center $R = \frac{1}{2}(r_1 + r_2)$ [see Eq. (19), where r_1 and r_2 are adjacent sites. However, the order parameters $\Delta_Q(r_i)$ given by the MC results are only defined at the sites r_i, not at the bond center R. In order to connect the MC data to the Hamiltonian, we interpolate $\Delta_Q(r_i)$ and take $\Delta_Q(R) = \frac{1}{2}(\Delta_Q(r_1) + \Delta_Q(r_2))$ at each bond (r_1, r_2). This interpolation process should be justified by the spatial smoothness of $\Delta_Q(r_i)$, at least within the PDW domains.
[106] K.-Y. Yang, T. M. Rice, and F.-C. Zhang, Phys. Rev. B **73**, 174501 (2006).
[107] J. P. F. LeBlanc, J. P. Carbotte, and E. J. Nicol, Phys. Rev. B **83**, 184506 (2011).
[108] T. M. Rice, K.-Y. Yang, and F. C. Zhang, Reports Prog. Phys. **75**, 016502 (2012).
[109] M. Hashimoto, I. M. Vishik, R.-H. He, T. P. Devereaux, and Z.-X. Shen, Nat. Phys. **10**, 483 (2014).
[110] I. M. Vishik, W. S. Lee, R.-H. He, M. Hashimoto, Z. Hussain, T. P. Devereaux, and Z.-X. Shen, New J. Phys. **12**, 105008 (2010).
[111] A. Greco and M. Bejas, Phys. Rev. B **83**, 212503 (2011).